JOURNAL OF GEOPHYSICAL RESEARCH, VOL. 112, B07307, doi:10.1029/2005JB003873, 2007

Crustal structure beneath the eastern margin of the Tibetan Plateau and its tectonic implications

Chun-Yong Wang,[1] Wei-Bin Han,[2] Jian-Ping Wu,[1] Hai Lou,[1] and W. Winston Chan[3]

Received 7 June 2005; revised 26 February 2007; accepted 26 March 2007; published 10 July 2007.

[1] Two crustal cross sections through the eastern margin of the Tibetan Plateau are jointly determined from deep seismic sounding. The E–W trending line AA' passes through the western Sichuan plateau (including the Songpan-Garze terrane and the Longmenshan fault belt) and ends in the Sichuan basin (a part of the Yangtze craton). Line BB' has a trend of NNE and crosses the Songpan-Garze terrane. Two-dimensional crustal structures along the profiles were jointly determined by the additional use of existing deep seismic sounding data. Our seismic velocity models indicate that the western Sichuan plateau and the Sichuan basin have crustal thicknesses of 62 and 43 km, average crustal *P* wave velocities of 6.27 and 6.45 km/s and lower crustal (V_p > 6.5 km/s) thicknesses of 27 and 15 km, respectively. Density models constructed from the seismic velocity models are consistent with observed Bouguer gravity anomalies. We infer that collision between the Tibetan Plateau and the Yangtze craton has caused thickening of the lower crust and uplift of the western Sichuan plateau. We detect a low-velocity layer in the upper crust of the western Sichuan plateau but observe no equivalence in the Sichuan basin; west dipping thrusts may detach into this low-velocity layer. The seismic phase P_mP in the western Sichuan plateau has low amplitude, suggesting high attenuation in the lower crust (Q_p of 100–300). We suggest that the high attenuation is a consequence of lower crustal flow caused by the large lower crustal thickness beneath the western Sichuan plateau.

Citation: Wang, C.-Y., W.-B. Han, J.-P. Wu, H. Lou, and W. W. Chan (2007), Crustal structure beneath the eastern margin of the Tibetan Plateau and its tectonic implications, *J. Geophys. Res.*, *112*, B07307, doi:10.1029/2005JB003873.

1. Introduction

[2] Continent-continent collision between the Indian and the Eurasian plates began at about 45 Ma, and has resulted in uplift of the Tibetan Plateau and major thickening of the underlying crust. Several models have been proposed to explain the mechanism of uplift and pattern of deformation for the Tibetan Plateau [e.g., *Molnar and Tapponnier*, 1975; *Tapponnier et al.*, 1982; *England and Houseman*, 1986]. Each of these models predicts different modes for the uplift and deformation of the Tibetan Plateau and in turn must explain the observed crustal and upper mantle structure [e.g., *Molnar and Chen*, 1978; *Chen and Molnar*, 1981; *Barazangi and Ni*, 1982; *Hirn et al.*, 1984; *Ni and Barazangi*, 1984; *Zhao et al.*, 1993; *Nelson et al.*, 1996; *Owens and Zandt*, 1997].

[3] Recent Global Positioning System (GPS) measurements of crustal motion in the central eastern Tibetan Plateau and its adjacent foreland indicate no significant shortening (<3 mm/yr) within the Longmenshan region, although it rises over 6 km within less than 100 km horizontal distance. The presence of active rock uplift along this margin is remarkable, given the distinct lack of upper crustal shortening between the plateau and the Sichuan basin [*Burchfiel et al.*, 1995; *Chen et al.*, 2000; *Zhang et al.*, 2004]. Some authors [e.g., *Block and Royden*, 1990; *Wernicke*, 1990; *Bird*, 1991; *Wdowinski and Axen*, 1992] proposed that in regions where the continental crust is hot, the middle or lower crust acts as a weak viscous layer capable of flow on geologic timescales. Thus lower crustal flow in the eastern margin of the Tibetan Plateau has been proposed as a mechanism by which the lateral pressure gradients within the crust are equilibrated, reducing variations in topography and crustal thickness [*Bird*, 1991; *Royden et al.*, 1997].

[4] Observations of crustal structure beneath the eastern margin of the Tibetan Plateau provide a test for tectonic models of the region and insight into the structure and kinematics of thickened continental crust. Several studies, including active source seismic refraction and wide-angle reflection experiments, referred to here as deep seismic sounding (DSS) experiments, have been carried out in the last 25 years [e.g., *Chen et al.*, 1986; *Xiong et al.*, 1986; *Cui et al.*, 1987, 1996], but existing data are sparse and remain inconclusive. In this paper, we present the results of DSS profiling conducted in 2001 (Figures 1 and 2a) across the

[1] Institute of Geophysics, China Seismological Bureau, Beijing, China.
[2] Sichuan Seismological Bureau, Chengdu, China.
[3] Multimax Inc., Herndon, Virginia, USA.

0148-0227/07/2005JB003873$09.00

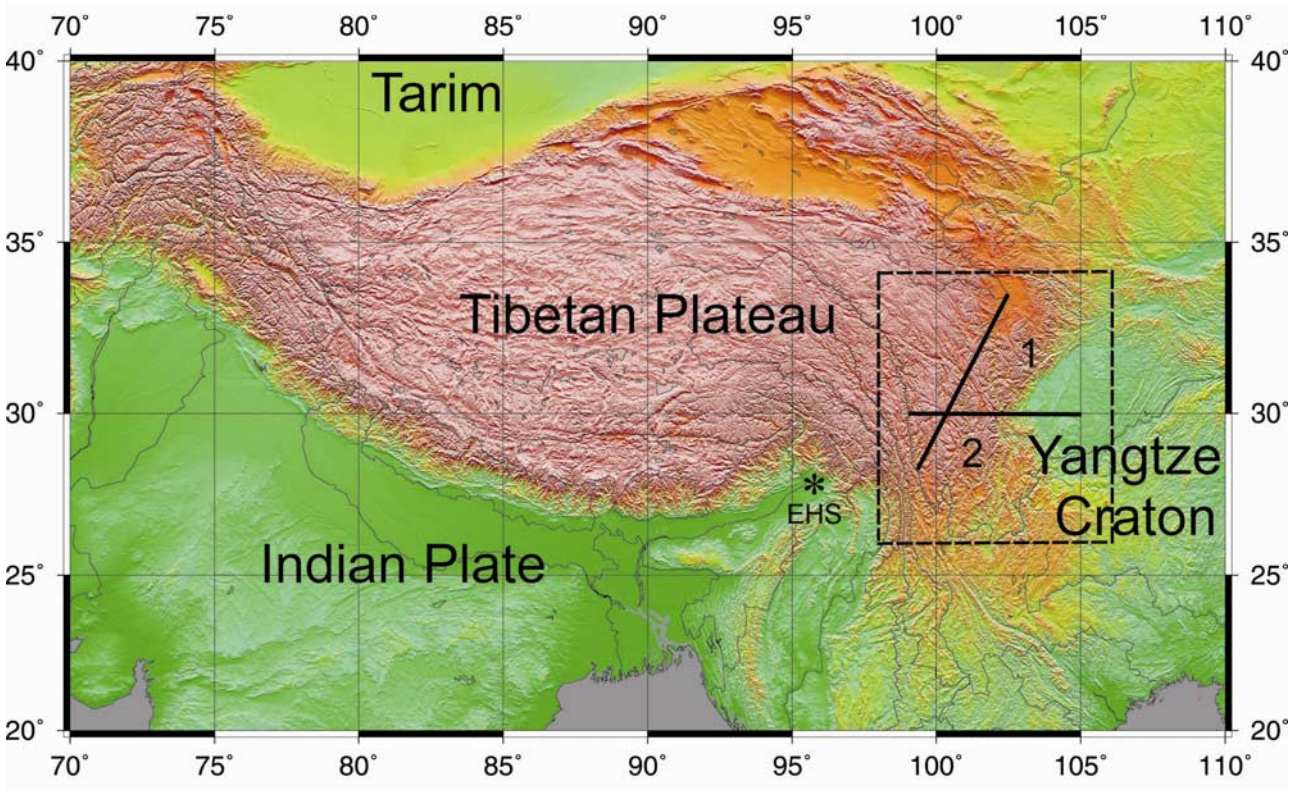

Figure 1. Topographic relief of the Tibetan Plateau and adjacent areas. Deep seismic sounding profiles are indicated by bold lines. The box indicates the study area depicted in Figure 2. The eastern boundary of the Tibetan Plateau is defined by 1, Longmenshan mountains; 2, Jinpingshan mountains. Asterisk denotes the location of the Eastern Himalayan Syntaxis (EHS).

western Sichuan plateau, which is the central eastern margin of the Tibetan Plateau, and the Sichuan basin.

2. Regional Geologic Setting and Previous Geophysical Results

2.1. Regional Geologic Setting

[5] The study area includes the western Sichuan plateau and the Sichuan basin. The western Sichuan plateau contains the Songpan-Garze terrane and the Longmenshan fault belt. The Sichuan basin is situated in the western Yangtze craton. The Longmenshan and Jinpingshan mountains are the east boundary of the Tibetan Plateau, with the Songpan-Garze terrane to the west and the Yangtze craton to the east (Figures 1 and 2a). The Yangtze craton has been in a stable sedimentary environment since late Paleozoic time, where thick sedimentary strata were deposited and have not been metamorphosed. During the Eocene and Oligocene, parts of the Yangtze craton have undergone folding [*Ren et al.*, 1999].

[6] Besides the Longmenshan fault belt, other fault zones in the study area include the Xianshuihe, Garze-Litang, Xiangcheng, Jinshajiang, and the Longriba faults in the western Sichuan plateau and Anninghe fault in the Yangtze craton (Figure 2a). The Xianshuihe fault is a strike-slip fault dated from at least the Quaternary period, and it extends from the Garze region through Daofu, to Kangding, with a length of about 450 km and northwest strike. The fault plane is inclined NE, with a dip angle of 60°−70° [*Sichuan Seismological Bureau*, 1989; *Allen et al.*, 1991]. The strike-slip rate on the Xianshuihe fault is 12 ± 4 mm/yr [*King et al.*, 1997; *Larson et al.*, 1999]. GPS measurements indicate that a crustal fragment rotates clockwise around the Eastern Himalayan Syntaxis (EHS, Figure 1), and that the block's eastern boundary is a sinistral fault system with a cumulative displacement rate of ~10 mm/yr relative to the South China Block [*Chen et al.*, 2000; *Zhang et al.*, 2004]. The eastern boundary of this crustal fragment is along the Xianshuihe/Xiaojiang fault system. Focal mechanism solutions of earthquakes occurring on the Xianshuihe fault indicate left-lateral strike-slip movement under east–west trending principal compressional stress [*Sichuan Seismological Bureau*, 1989]. The Jinshajiang fault is the west boundary of the Songpan-Garze terrane, with the Sanjiang tectonic zone farther to the west. The north–south trending Anninghe fault is situated along the southwest margin of the Yangtze craton. The Panxi tectonic zone (100 km wide and 300 km long) is distributed along the Anninghe fault zone, with anomalous deep geophysical structures and rich mineral resources [*Cui et al.*, 1987; *Teng*, 1994].

[7] The eastern margin of the Tibetan Plateau, i.e., the transitional zone between the Tibetan Plateau and Yangtze craton has experienced strong crustal deformation and faulting during both the Mesozoic and late Cenozoic epochs [*Chen et al.*, 1994; *Burchfiel et al.*, 1995; *Kirby et al.*, 2002, 2003]. The first event produced the folding in the Songpan-Garze terrane, local metamorphism in the east of the terrane, and was associated with plutonic activity. The second event

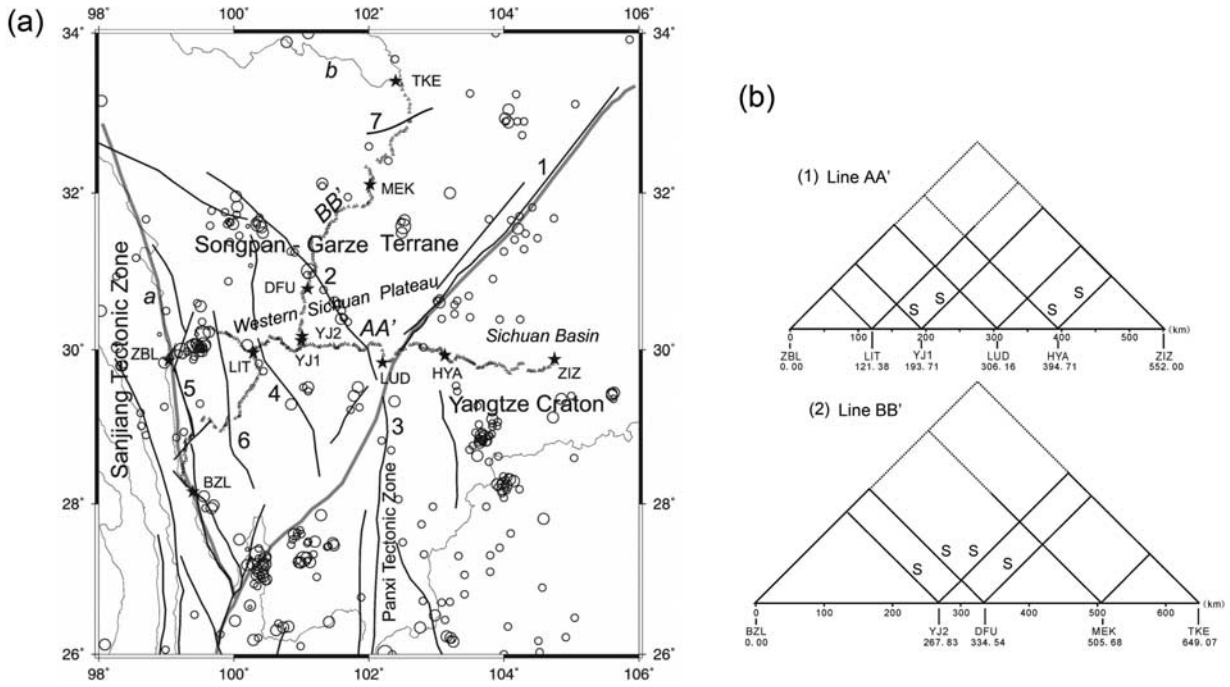

Figure 2. (a) Geologic setting of the study area and locations of new seismic sounding profiles. Seismic stations are indicated by open triangles: AA' is the Zhubalong-Zizhong profile, and BB' is the Benzilan-Tangke profile. Stars denote position of shot points. Grey lines mark boundaries between tectonic units. Faults are indicated by bold lines with number: 1, Longmenshan fault; 2, Xianshuihe fault; 3, Anninghe fault; 4, Garze-Litang fault; 5, Jinshajiang Fault; 6, Xiangcheng fault; 7, Longriba fault. Rivers are indicated by thin lines: a, Jingshajiang River; b, Yellow River. Circles denote earthquakes with $M > 5.0$ since 1960. (b) Layout of the observation (1) line AA' and (2) line BB'. Shot points are located according to their projection onto straight lines. Numbers beneath shot point indicate the distance from the shot point to the western end of line AA', or the southern end of line BB'. Dashed lines denote records with no useful information. The ones denoted by "S" have the record sections presented in the auxiliary material.

appears much weaker than the first with only minor crustal shortening evidence but significant uplift of the plateau [*Clark and Royden*, 2000].

[8] Earthquakes regularly occur in the western Sichuan plateau (Figure 2a). Significant historic events include those at Litang (M 7.2) in 1954, Kangding (M 7.5) in 1955, Zhuwei (M_s 6.8) in 1967, Luhuo (M_s 7.9) in 1973, Songpan (M_s 7.2) in 1976, and Daofu (M_s 6.9) in 1981 [*Gu*, 1983; *Sichuan Seismological Bureau*, 1989; *Jones et al.*, 1984; *Allen et al.*, 1991; *Papadimitriou et al.*, 2004].

2.2. Previous Geophysical Studies

[9] Crustal and upper mantle structures beneath the eastern margin of the Tibetan Plateau and its surrounding areas were previously outlined by several DSS profiles (Figure 3). Near Longmenshan, the crustal thickness varies sharply from about 40 km in the Yangtze craton to 53 km in the Songpan-Garze terrane [*Chen et al.*, 1986]. The Huashixia-Shaoyang profile [*Cui et al.* 1996] shows that the crustal structure to the north of the western Sichuan plateau, with a crustal thickness of about 60 km, is quite different from that presented by *Chen et al.* [1986]. The Lijiang-Zhehai profile [*Xiong et al.*, 1986] indicates that the crustal structure of the Panxi tectonic zone, situated to the southwest of the Sichuan basin, is characterized by a low-velocity layer in the middle crust (5.6 to 6.0 km/s) and a low-velocity anomaly in the upper mantle (7.7 to 7.9 km/s). The Lijiang-Xinshizhen and the Lazha-Changheba profiles provide supporting evidence for a low-velocity layer in the middle crust and a low-velocity anomaly in the uppermost mantle in the Panxi tectonic zone [*Cui et al.*, 1987]. In addition, the Simao-Zhongdian profile in western Yunnan shows that the crustal thickness in northwestern Yunnan, about 70 km south of the western Sichuan plateau, is 58 km [*Lin et al.*, 1993]. After collecting the arrival time data from a large industrial explosion (10^7 kg TNT) and 154 local earthquakes, recorded at 50 seismic stations in the Sichuan and Yunnan regions, *Zhao and Zhang* [1987] presented one-dimensional (1-D) P wave velocity models of the western Sichuan plateau with a crustal thickness of 61 to 64 km and a P_n velocity of 7.80 to 7.84 km/s, as well as models of the Sichuan basin that have a crustal thickness of 40 to 41 km and a P_n velocity of 8.15 to 8.20 km/s.

[10] The 3-D velocity structure of the crust and upper mantle in southwestern China has been determined from traveltime data collected by regional seismic networks in the Sichuan and Yunnan regions [e.g., *Liu et al.*, 1989; *Sun et al.*, 1991; *Huang et al.*, 2002; *Wang et al.*, 2003]. *Wang et al.* [2003] demonstrate that a positive anomaly (2 to 4%) and a large-scale negative anomaly (3 to 5%) of P wave velocity exist in the upper crust of the Sichuan basin and the western Sichuan plateau, respectively. The transition

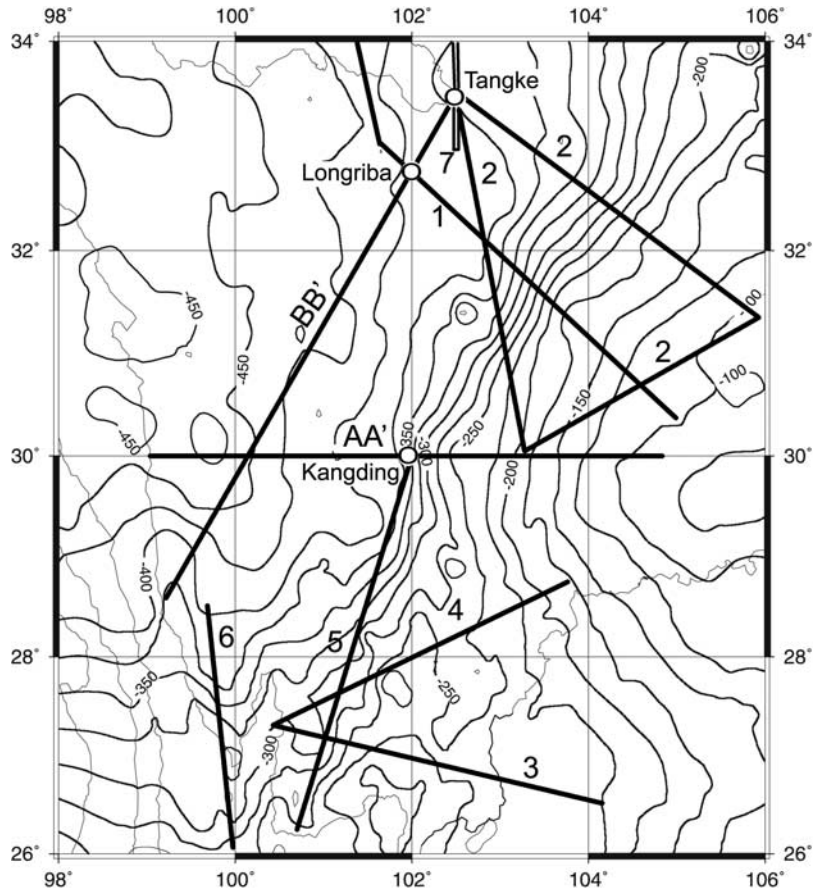

Figure 3. Bouguer gravity anomalies and the location of the DSS and deep seismic reflection profiles in the study area. Contour interval is 25 mGal. The Longmenshan fault belt is manifested as a large-scale gravity gradient belt trending NNE. Seismic profiles are indicated by straight lines and with numbers or letters: 1, Huashixia-Shaoyang profile; 2, Longmenshan triangle; 3, Lijiang-Zhehai; 4, Lijiang-Xinshizhen; 5, Lazha-Changheba; 6, Simao-Zhongdian; 7, Hezuo-Tangke. AA', Zhubalong-Zizhong; BB', Benzilan-Tangke.

between these positive and negative anomalous areas coincides with the Longmenshan fault belt. Strike-slip faults, such as the Xianshuihe and Anninghe faults, are associated with local negative *P* wave velocity anomalies in the upper crust. Regionally, the crustal and the upper mantle structures in southwestern China are characterized by relatively low crustal *P* wave velocities, low P_n velocities and large crustal thickness variations.

[11] There is a 350 mGal difference of Bouguer gravity anomaly between the western Sichuan plateau and the Sichuan basin [*Yuan*, 1996]. A NNE trending zone of high gravity gradient, approximately 150 km wide and 900 km long, coincides with the Longmenshan fault belt [*Li*, 1993]. The gravity field varies gradually between the Longmenshan fault belt and the Jinshajiang fault belt (Figure 3).

[12] Heat flow values determined in the Songpan-Garze terrane range from 36 to 87 mW/m^2, with an average value of 62 ± 16 mW/m^2, and values in the western Sichuan–central Yunnan area range from 53 to 107 mW/m^2, with an average value of 76 ± 13 mW/m^2 [*Hu et al.*, 2000]. Hot springs are distributed along the Xianshuihe, the Garze-Litang and the Anninghe faults. Most of the springs have temperatures above 40°C, with several above 80°C [*Teng*, 1994].

3. Crustal Velocity Structures in the Study Area

3.1. Layout of the DSS Profiles

[13] Our DSS project in the study area involves two intersecting profiles (line AA' and line BB') with an overlapping portion from Litang to Yajiang (Figure 2a). Line AA' trends along latitude 30°N. It begins at Zhubalong (ZBL) close to the Jinshajiang River, passes through Litang (LIT), Yajiang (YJ1), Kangding, Luding (LUD), Hongya (HYA), and ends at Zizhong (ZIZ), with a total length of 552.02 km. Line AA' passes through the Songpan-Garze terrane, the Longmenshan fault belt, and the Yangtze craton, and joins the northern end of the Lazha-Changheba profile [*Cui et al.*, 1987] at Kangding. Line BB' extends from Benzilan (BZL) close to the Jinshajiang River, through Xiangcheng, Litang, Yajiang (YJ2), Daofu (DFU), Ma'erkang (MEK), and to Tangke (TKE) by the Yellow River, with a NNE trend and a total length of 649.07 km. Line BB' passes through the Songpan-Garze terrane and crosses the Huashixia-Jianyang profile [*Cui et al.*, 1996] at Longriba (Figure 3).

Table 1. Location of Shot Points and Their Shot Charges

Line	Shot Name	Code	Latitude N	Longitude E	Altitude, m	Charge, kg
AA'	Zhubalong	ZBL	29° 52.15′	99° 02.22′	2500	2500
AA'	Litang	LIT	29° 57.68′	100° 17.38′	3940	3000
AA'	Yajiang	YJ1	30° 10.56′	101° 00.84′	2630	2500
AA'	Luding	LUD	29° 50.57′	102° 12.34′	1270	2000
AA'	Hongya	HYA	29° 55.97′	103° 07.40′	530	2500
AA'	Zizhong	ZIZ	29° 53.07′	104° 45.09′	310	2500
BB'	Benzilan	BZL	28° 09.38′	99° 23.76′	2030	2500
BB'	Yajiang	YJ2	30° 07.34′	100° 59.81′	2630	2500
BB'	Daofu	DFU	30° 47.08′	101° 05.51′	2990	2000
BB'	Maerkang	MEK	32° 06.54′	102° 01.04′	2490	2500
BB'	Tangke	TKE	33° 24.43′	102° 23.85′	3450	4000

[14] The DSS profiles utilize 11 explosions (Table 1). All explosions were fired underwater at a local water depth of 8–15 m, except shot LIT, which is a borehole explosion at a local depth of 30 m, and with charge distributed among 20 holes. Shots ZBL and BZL are located at the western and southwestern boundaries of the Songpan-Garze terrane, respectively, whereas MEK and TKE lie in the northern Songpan-Garze terrane. LIT situates along the Garze-Litang fault belt. LUD and DFU are along the Xianshuihe fault belt. YJ1 and YJ2 are located between the Garze-Litang fault and the Xianshuihe fault. HYA lies in the west Sichuan basin, ~60 km east to the Longmenshan fault belt, and ZIZ lies in the central Sichuan basin (Figure 2).

[15] The seismic waves excited by all explosions were recorded by a total of about 220 three-component short-period digital seismographs (with maximum gain at 1 Hz), which were successively deployed along line AA' and line BB', with recorder interval of 2 to 4 km. All recorders and shots were synchronized through GPS clocks. The sampling interval on records is 10 ms. Timing errors of recorders and explosions are less than 0.01 s. The profiles are crooked (Figure 2a), but a 2-D velocity structure along each profile was assumed. The observation system is online, reversed and overlapped (Figure 2b). On the abscissas of distance, shot points ZBL, LIT, YJ1, LUD, HYA, and ZIZ on line AA' are located at 0.00, 121.38, 193.71, 306.16, 394.71, and 552.02 km, respectively. Shot points BZL, YJ2, DFU, MEK, and TKE on line BB' are located at 0.00, 267.83, 334.54, 505.68, and 649.07 km, respectively. The low-pass-filtered (8 Hz) record sections along lines AA' and BB' were plotted with a reduced velocity of 6.0 km/s (Figures 4–10 and the auxiliary material) and were interpreted shot by shot. The 2-D crustal velocity structures along lines AA' and BB' were jointly determined.[1]

3.2. General Analysis of Seismic Phases

[16] Our seismic phase identification and analysis is based on the assumption that the crust is horizontally layered and that seismic velocity generally increases with depth [*Meissner*, 1986]. On the record sections, seismic phases P_g and P_mP can be directly identified. The first arrival phase P_g is the head wave or diving wave propagating within the crystalline basement, and P_mP is the Moho reflection. The distance range for observing phase P_g is from approximately 20 to 100 km. The critical distance of phase P_mP varies from 140 to 180 km. The P_n phase is refracted through the uppermost mantle and can be identified as the first arrival beyond about 200 km. Besides phases P_g, P_mP and P_n, there are 3 or 4 crustal reflection phases, which can be traced as secondary arrivals on the record sections. In the order of arrival times, these phases are labeled as P_1, P_2, P_3, and P_4 in the western Sichuan plateau, and are labeled as P_1, P_3 and P_4 in the Sichuan basin, which is also related to the record sections of shots ZIZ, HYA and LUD (the eastern branch). After picking the arrival times of various phases on the record section of each shot, we applied topographic corrections to them for a reference elevation of 3000 m. The corrected traveltimes were used to calculate the mean velocity of the reflection phases and apparent velocity of the refraction phases [*Giese and Prodehl*, 1976; *Sheriff and Geldart*, 1995]. The topographic correction is calculated by

$$\Delta t = -(H_s + H_o) \times \sqrt{U_r^2 - U_a^2}$$

where $H_s = H_{sp} - H_r$, $H_o = H_{st} - H_r$, H_{sp} is the elevation of shot point, H_{st} is the elevation of station, and H_r is the reference elevation; $U_r = 1/V_r$, $U_a = 1/V_a$, V_r is the average velocity of the layer above reference elevation, and V_a is the horizontal apparent velocity of the phase at the station, as evaluated from the traveltime curve of the phase. Record sections used in the analysis are shown in Figures 4–10 and the auxiliary material Figures S1 to S4, with dashed lines delineating interpreted phases.

3.2.1. Line AA'

3.2.1.1. Shot ZBL (Zhubalong)

[17] Shot ZBL was a 2500 kg underwater explosion fired in the Jinshajiang River. On the record section (Figure 4), P_g has an apparent velocity of 5.90 km/s at distances from 30 to 60 km. Phase P_1 is weak. P_2 is a fairly strong phase, traceable from 60 to 140 km and a mean velocity of 5.98 km/s. P_3 is a distinct phase at distances from 140 to 200 km with a mean velocity of 6.18 km/s. P_4 is traceable from 160 to 210 km. Phase P_mP is weak and P_n is not clearly observable.

3.2.1.2. Shot LIT (Litang)

[18] Shot LIT was a borehole 3000 kg explosion near the town of Litang. In the western branch (Figure 5a), P_g has a low apparent velocity of 5.85 km/s at distances less than 50 km. P_1 can be traced at distances from 40 to 85 km. P_2 is a distinct phase traceable from 70 to 122 km, with a mean velocity of 5.93 km/s. P_3 can be traced at distances from 90

[1] Auxiliary materials are available in the HTML. doi:10.1029/2005JB003873.

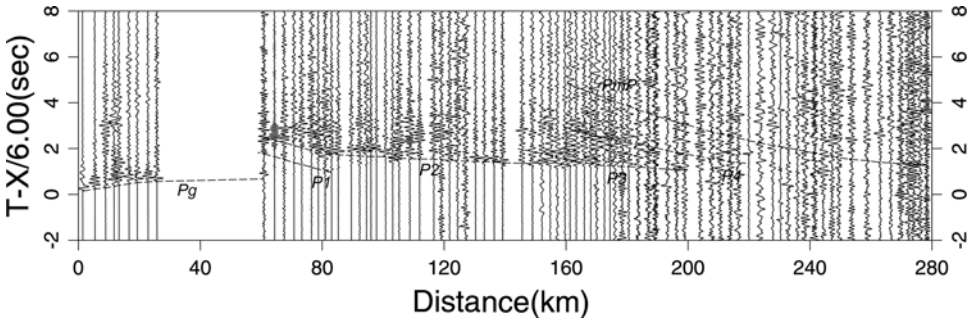

Figure 4. Trace-normalized low-pass-filtered (8 Hz) record section of shot ZBL with reduced velocity 6.0 km/s. For this and all other record sections (Figures 5 to 10), the interpretive phase lines are described in the main text.

to 122 km. Because of the limited observation distances (less than 122 km), P_4, P_mP and P_n are not observed.

[19] In the eastern branch (Figure 5b), P_g has an apparent velocity of 5.85 km/s at distances from 30 to 80 km. P_1 can be traced from 60 to 120 km, with a mean velocity of 5.90 km/s. P_2 is a dominant phase traceable from 80 to 150 km with a mean velocity of 5.93 km/s. P_3 is distinct at distances from 120 to 200 km and has a mean velocity of 6.15 km/s. P_mP is distinct from 165 to 250 km with a mean velocity of 6.30 km/s. P_4 is weak and P_n is not clearly observable.

3.2.1.3. Shot YJ1 (Yajiang 1)

[20] Shot YJ1 was a 2500 kg underwater explosion in the Yalongjiang River. In the western branch, P_g has an apparent velocity of 6.00 km/s at distances from 25 to 60 km. P_1 is weak but traceable from 50 to 100 km. P_2 is a distinct phase from 60 to 120 km and has a mean velocity of 5.90 km/s. P_3 can be traced at distances from 120 to 180 km with a mean velocity of 6.08 km/s. P_4 is weak and P_mP and P_n are not observed.

[21] In the eastern branch, there exists large background noise beyond 90 km. However, besides P_g, which is distinct for distances up to 70 km and has an apparent velocity of 5.95 km/s, P_1 and P_2 can be traced from 70 to 130 km and 100 to 170 km with mean velocities of 6.12 km/s and 6.10 km/s, respectively. P_3 is traceable from 120 to 185 km. P_mP is weak, but can be traced from 160 to 240 km, maintaining a mean velocity of 6.36 km/s. P_4 is weak and P_n is not clearly observable.

3.2.1.4. Shot LUD (Luding)

[22] Shot LUD was a 2000 kg underwater explosion in the Daduhe River. In the western branch (Figure 6a), P_g has an apparent velocity of 5.95 km/s at distances up to 80 km. P_1 has a mean velocity of 5.95 km/s at distances from 60 to 110 km. P_2 is distinct from 70 to 140 km with a mean

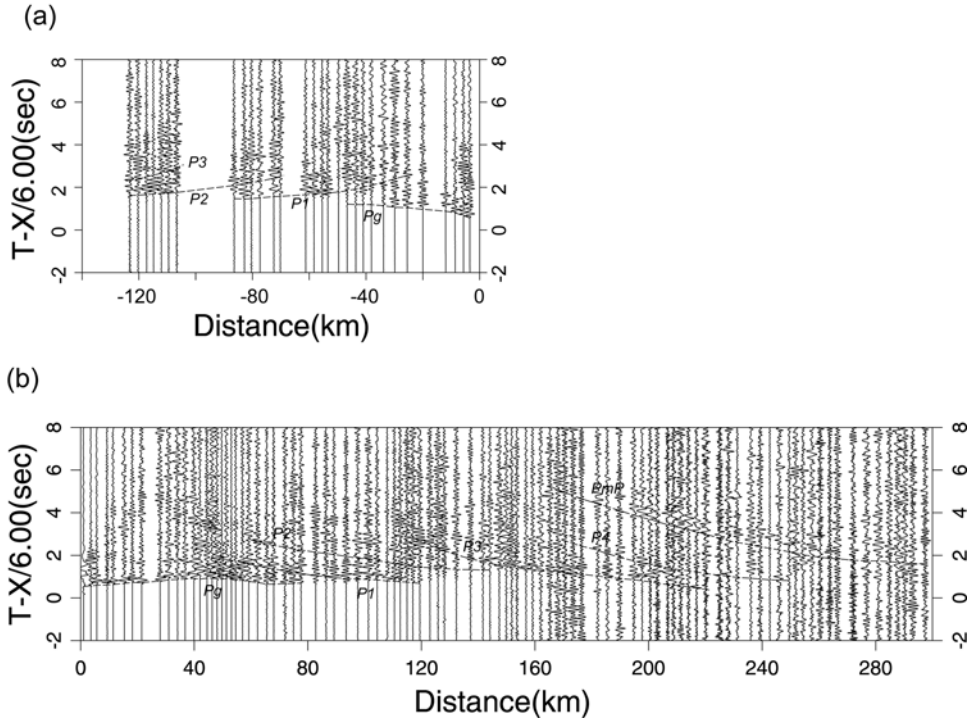

Figure 5. (a) Trace-normalized low-pass-filtered (8 Hz) record section of shot LIT (the western branch). (b) Trace-normalized low-pass-filtered (8 Hz) record section of shot LIT (the eastern branch).

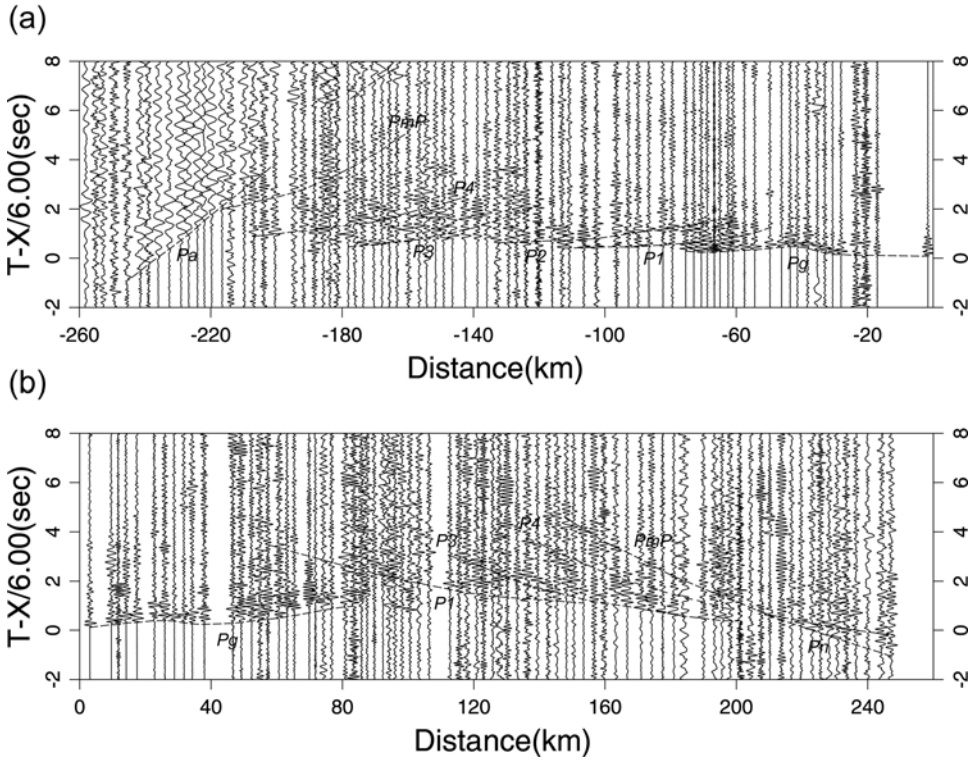

Figure 6. (a) Trace-normalized low-pass-filtered (8 Hz) record section of shot LUD (the western branch). (b) Trace-normalized low-pass-filtered (8 Hz) record section of shot LUD (the eastern branch).

velocity of 6.02 km/s. P_3 is traceable at distances from 120 to 180 km, with a mean velocity of 6.20 km/s. P_4 can be traced from 150 to 190 km. A strong seismic phase P_a with low frequency (1.0 to 1.5 Hz) and high apparent velocity (13.0 to 15.0 km/s) appears beyond 160 km. P_mP is weak and P_n is not observed.

[23] The appearance of seismic phases along the eastern branch (Figure 6b) is quite different from that along the western branch. Along the eastern branch, P_g has an apparent velocity of 6.05 km/s at distances up to 60 km. P_1 and P_3 can be traced from 70 to 140 km and 110 to 170 km with mean velocities of 6.05 km/s and 6.15 km/s, respectively. P_2 is not observed. P_4 is distinct at distances from 130 to 190 km, with a mean velocity of 6.35 km/s. P_mP can be traced at distances from 140 to 250 km, with a mean velocity of 6.50 km/s. P_n is distinct beyond 200 km, with an apparent velocity of 8.12 km/s.

3.2.1.5. Shot HYA (Hongya)

[24] Shot HYA was a 2500 kg underwater explosion in the Minjiang River. Except for P_g, the traceable distances of all other phases are obviously shorter than they are on the record sections of other shots in this survey. This difference was probably caused by a unique geological environment or by an incomplete explosion. In the western branch, P_g is the first arrival at distances less than 60 km. P_1 is traceable at distances from 50 to 90 km and has a mean velocity of 6.01 km/s. P_2 is traceable at distances from 70 to 110 km, and has a mean velocity of 6.05 km/s. P_3 is distinct from 100 to 160 km, with a mean velocity of 6.13 km/s. P_4 is weak, but can be traced from 135 to 185 km. P_mP and P_n are not clearly observable.

[25] In the eastern branch, P_g has a lower apparent velocity of 5.75 km/s at distances up to 60 km. P_1 is not clear and P_2 is not observed. P_3 can be traced from 70 to 130 km, and has a mean velocity of 6.05 km/s. P_4 is distinct from 85 to 140 km, with a mean velocity of 6.18 km/s. P_mP is traceable from 105 to 160 km, with a mean velocity of 6.48 km/s.

3.2.1.6. Shot ZIZ (Zizhong)

[26] Shot ZIZ was a 2500 kg underwater explosion in a local river. On the record section (Figure 7), P_g has a low apparent velocity of 5.85 km/s at distances less than 100 km. P_1, P_3 and P_4 can be traced with mean velocities of 6.05, 6.16, and 6.40 km/s, respectively. P_2 is not observed. P_mP is a dominant phase with strong amplitude from 130 to 240 km, and has a high mean velocity (6.50 km/s). P_n appears beyond 180 km and has high apparent velocity of 8.15 km/s.

3.2.2. Line BB'

3.2.2.1. Shot BZL (Benzilan)

[27] Shot BZL was a 2500 kg underwater explosion in the Jinshajiang River. On the record section (Figure 8), P_g has a high apparent velocity of about 6.18 km/s from 20 to 80 km. P_1 and P_2 can be traced at distance from 50 to 110 km and from 60 to 130 km, and has mean velocities of 6.10 and 6.12 km/s, respectively. P_3 is distinct from 100 to 160 km and has a mean velocity of 6.25 km/s. P_4 is weak. P_mP can be traced from 140 to 230 km, with a mean velocity of 6.35 km/s. P_n is not clearly observable.

3.2.2.2. Shot YJ2 (Yajiang 2)

[28] Shot YJ2 was a 2500 kg underwater explosion in the Yalongjiang River. In the southern branch, P_g has an apparent velocity of 6.02 km/s at distances from 20 to

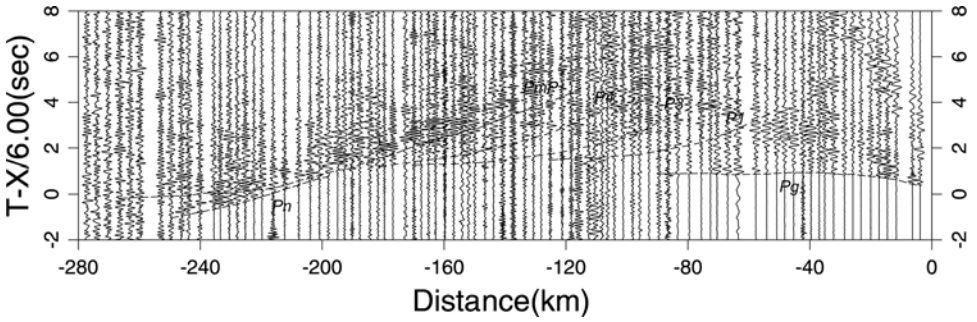

Figure 7. Trace-normalized low-pass-filtered (8 Hz) record section of shot ZIZ.

70 km. P_1 and P_2 can be traced with mean velocities of 6.05 and 6.08 km/s at distances from 40 to 80 km and from 60 to 130 km, respectively. P_3 and P_4 can be traced and have mean velocities of 6.15 and 6.25 km/s, respectively. P_mP and P_n are not clearly observable.

[29] In the northern branch, P_g has an apparent velocity of 6.08 km/s at distances from 20 to 80 km. P_1 and P_2 have mean velocities of 6.08 and 6.03 km/s, respectively. P_3 is distinct from 100 to 170 km, with a mean velocity of 6.15 km/s. P_4 is traceable from 120 to 200 km, with a mean velocity of 6.25 km/s. P_mP and P_n are not clearly observable.

3.2.2.3. Shot DFU (Daofu)

[30] Shot DFU was a 2000 kg underwater explosion in the Xianshuihe River. In the southern branch, P_g has an apparent velocity of 6.05 km/s at distances from 20 to 80 km. P_1 and P_2 can be traced with low mean velocities of 6.05 and 6.07 km/s, respectively. P_3 and P_4 have mean velocities of 6.15 and 6.25 km/s, respectively. P_mP is traceable from 140 to 210 km, with a mean velocity of 6.30 km/s. P_n is not clearly observed.

[31] In the northern branch, P_g has an apparent velocity of 6.05 km/s at distances from 20 to 70 km. The reduced time-distance curve of phase P_g has an arc shape, which implies the presence of a low-velocity zone with small local extent close to the Xianshuihe fault belt. P_1 is weak. P_2 and P_3 have mean velocities of 6.05 km/s and 6.15 km/s at distances from 60 to 90 km and from 80 to 150 km, respectively. P_4 is weak. P_mP is distinct at distances from 150 to 220 km with a mean velocity of 6.36 km/s. P_n is not clearly observable.

3.2.2.4. Shot MEK (Ma'erkang)

[32] Shot MEK was a 2500 kg underwater explosion in the Daduhe River. In the southern branch (Figure 9a), P_g has an apparent velocity of 5.90 km/s at distances from 20 to 70 km. P_1 and P_2 can be traced from 70 to 125 km, respectively, with the same mean velocity of 6.05 km/s. P_3 is distinct at distances from 110 to 150 km, with a mean velocity of 6.20 km/s. P_4 has a mean velocity of 6.25 km/s. P_mP is traceable at distances from 150 to 260 km, with a mean velocity of 6.30 km/s. P_n is not clear. A distinct seismic phase P_b with low apparent velocity (5.20 km/s) and relatively high energy appears at distances from 125 to 170 km.

[33] In the northern branch (Figure 9b), P_g has a low apparent velocity (5.65 km/s) at distances up to 80 km. P_1 can be traced from 60 to 120 km with a mean velocity of 5.95 km/s. P_2 is distinct at distances from 80 to 150 km and has a mean velocity of 5.90 km/s. P_3 is traceable from 80 to 150 km with a mean velocity of 6.15 km/s. Because of limited distance (150 km), phases P_4, P_mP and P_n were not observed.

3.2.2.5. Shot TKE (Tangke)

[34] Shot TKE was a 4000 kg underwater explosion in the Yellow River. On the record section (Figure 10), P_g has a low apparent velocity (5.60 km/s), which is consistent with the northern branch of shot MEK. P_1 has a low mean velocity of 5.85 km/s. P_2 is weak. P_3 is distinct at distances from 120 to 180 km with a mean velocity of 6.15 km/s. P_4 has a mean velocity of 6.20 km/s. P_mP is traceable from 170 to 280 km, with a mean velocity of 6.25 km/s. P_n is not clearly observable.

4. The 2-D Velocity and Density Structure

4.1. Interpretation Methods of DSS Data

[35] The 2-D interpretation of seismic wide-angle reflection/refraction data generally consists of two steps, iterative

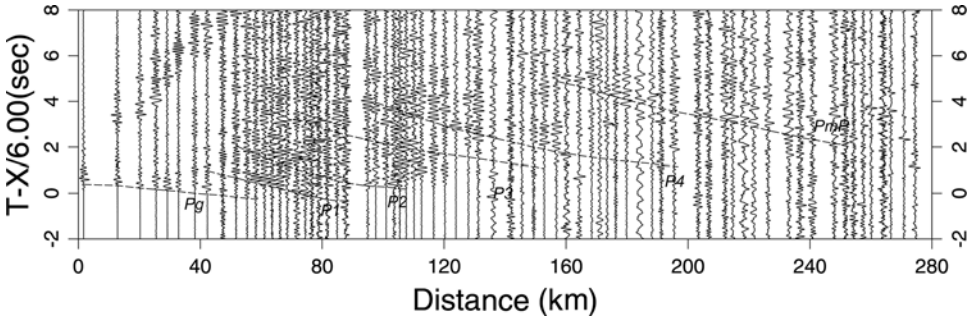

Figure 8. Trace-normalized low-pass-filtered (8 Hz) record section of shot BZL.

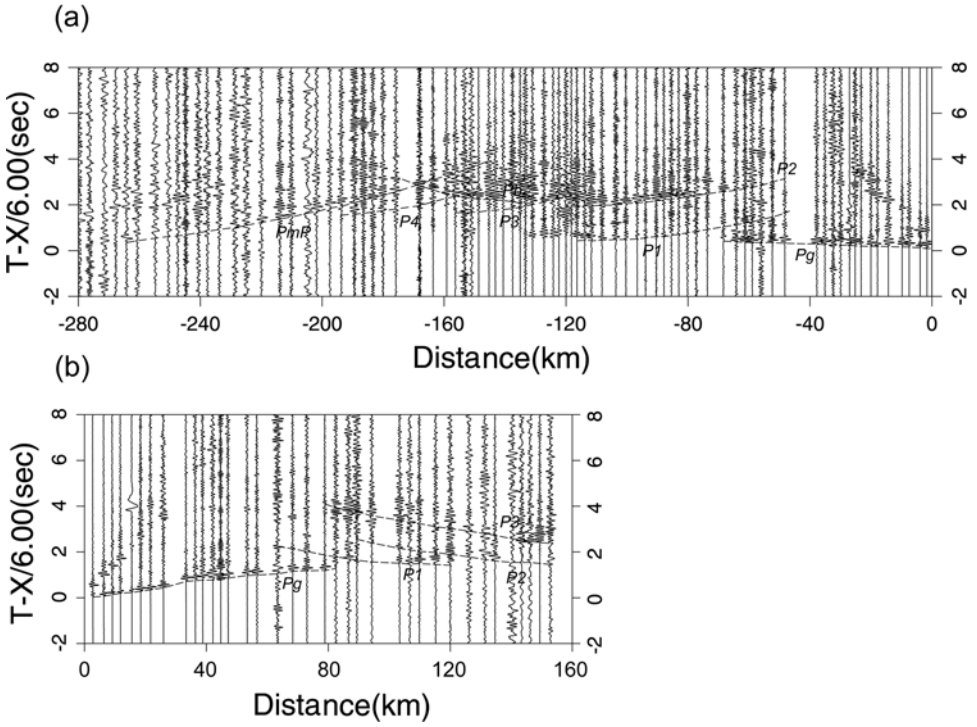

Figure 9. (a) Trace-normalized low-pass-filtered (8 Hz) record section of shot MEK (the southern branch). (b) Trace-normalized low-pass-filtered (8 Hz) record section of shot MEK (the northern branch).

forward fitting of traveltimes and amplitude on seismic record sections [*Giese and Prodehl*, 1976; *Meissner*, 1986; *Mooney*, 1989; *Mooney and Braile*, 1989; *Holbrook et al.*, 1992], and construction of a velocity model with a layered crust with velocities varying laterally and generally increasing with depth [*Meissner*, 1986]. The concurrent portion between LIT (Litang) and YJ1 (Yajiang) along line AA' and line BB' creates a coincidence constraint that produces the necessity to jointly determine the 2-D velocity structure along the two profiles. On the basis of phase identification and traveltime corrections on the record sections of the 11 shots of the two profiles, the 2-D velocity structure was determined using the trial-and-error method [*Gajewski and Prodehl*, 1987]. The seismic record sections were simulated using the theory of asymptotic rays [*Cerveny et al.*, 1977]. In general, the topographic corrections of traveltimes improve the fit of the data to a relatively simple model.

[36] The first arrival in the upper crust (i.e., P_g) can be interpreted by tomography of a diving wave, e.g., the finite difference traveltime inversion [*Vidale*, 1988; *Hole*, 1992; *Ammon and Vidale*, 1993] and the damped least squares [*Lutter et al.*, 1999], so as to obtain the 2-D velocity structure of the upper crust. The number of rays traveling through each cell is used to assess the resolution of inversion [*Hole*, 1992; *Parsons et al.*, 1996]. *Wang et al.* [2000] applied the finite difference traveltime inversion to DSS data in eastern China.

[37] On the basis of the traveltimes of all the phases on record sections, and referring to a 2-D velocity model of upper crust, which was obtained from the finite difference traveltime inversion of the first arrival, the 1-D velocity models are determined for the record section of each branch

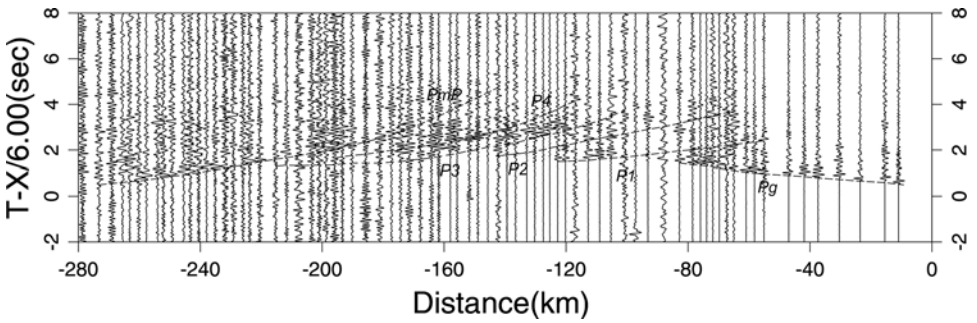

Figure 10. Trace-normalized low-pass-filtered (8 Hz) record section of shot TKE.

by using ray tracing and synthetic seismogram methods [*Fuchs and Mueller*, 1971; *Braile and Smith*, 1975; *Sandmeier and Wenzel*, 1986]. However, 1-D models are limited by the assumption of lateral homogeneity. On the basis of the 1-D models and the layout of profiles (Figure 2b), we constructed two 2-D initial velocity models along lines AA' and BB'. The ray tracing method was used to fit the traveltimes of the reflection and refraction phases, and ray synthetic seismograms [*Cerveny and Psencik*, 1984] were used to constrain the amplitudes of the phases. Improvements were made to the 2-D velocity model using the trial-and-error method until the RMS values of traveltime residuals could not be reduced.

4.2. Crustal Structures on the Basis of DSS Data

4.2.1. The 2-D Velocity Structures in the Upper Crust From Finite Difference Traveltime Inversion

[38] First arrival times were collected from recordings of six shots on line AA' and five shots on line BB', whereby a total of 470 arrival times were recorded along line AA' and 379 along line BB'. The inversion model was parameterized via rectangular cells of dimension 5 km (horizontal) × 2 km (vertical) on each profile. To maintain accuracy, a uniform 1-km square grid was used for the traveltime calculation. The finite difference traveltime inversion method was used, and the final velocity model was obtained after 5 iterations for each profile. The initial 1-D upper crustal model was obtained by averaging the 1-D models deduced from P_g arrival times interpreted from each record along the profile. The RMS traveltime residuals on lines AA' and BB' are 0.69 s and 0.62 s for the initial 1-D models and decrease to 0.19 s and 0.21 s for the final 2-D models, respectively. There is no significant difference between the models obtained after 5 and 10 iterations for both profiles. Meanwhile, we calculated the number of P_g rays traveling through each cell, which is used to assess the resolution of the inversion. The final 2-D velocity model of the upper crust and the number of P_g rays traveling through each rectangular cell along line AA' and line BB' are illustrated in Figure 11.

[39] Figure 11a shows three low-velocity zones near the surface along line AA'. These zones are situated on the east side of HYA, around LUD, and on the west side of LIT, respectively, among which the Sichuan basin has sediments of about 6 km in thickness. The crystalline basement near YJ1 has been uplifted. Using the geological survey [*Xu et al.*, 1992] and the velocity isolines in this study, we inferred the location of the Garze-Litang fault and the Longmenshan fault on the 2-D model of the upper crust. Ray penetration depths reach 18 km over much of the profile and >10 rays typically pass through each cell at these depths (Figure 11).

[40] Along line BB', an uplift of crystalline basement and a high-velocity anomaly exists at a depth of 2 km in the region between BZL and the Xiangcheng fault, and in the region between YJ2 and DFU (Figure 11c). The velocity is as high as 6.20 km/s at 40 km to the north of BZL. Low-velocity zones exist near the surface in the region between the Xiangcheng fault and the Garze-Litang fault, and in the region between MEK and TKE. The Longriba fault, at about 35 km to the north of MEK, is located in the southern boundary of the low-velocity zone between MEK and TKE. The penetrating depth of seismic rays is shallow (about 6 km) beneath BZL and DFU. Beneath other shots, the penetrating depth is up to 10 km. At those depths, the number of rays traveling through the cells is mostly greater than 5 (Figure 11d).

4.2.2. Final 2-D Crustal Structure

[41] Figures 12a and 12b show the final 2-D crustal velocity models along lines AA' and BB'. The crustal structure of the eastern portion of line AA' is jointly determined by the traveltime data of phases on the record sections of shot ZIZ (Figure 7) and the eastern branch of shots HYA and LUD (Figure 6b), whereas the crustal structure of the western portion is jointly determined by shot ZBL (Figure 4), shot LIT (Figures 5a and 5b), and the western branch of shots YJ1 and LUD (Figure 6a). The crustal structure of the northern portion of line BB' is jointly determined by the traveltime data of phases on the record sections of shot TKE (Figure 10), shot MEK (Figures 9a and 9b), and the northern branch of shots DFU and YJ2 whereas the crustal structure of the southern portion is jointly determined by shots BZL (Figure 8) and YJ2, and the southern branch of shot DFU.

[42] In the crustal structure models shown in Figures 12a and 12b, the lower interface of layer i is defined primarily by phase P_i, the corresponding interface is labeled C_i, and the bold lines denote regions of reflection for phases P_i (i = 1, 2, 3, 4) and P_mP. The Moho is the lower interface of layer 5. The concept of seismic lower crust stems from the work of *Conrad* [1925], who discovered a layer above the Moho that subsequently came to be identified as a basaltic layer with a velocity of about 6.50 km/s, underlying a supposedly ubiquitous Conrad discontinuity [*Jeffreys*, 1926]. Although the definition of seismic lower crust is more flexible today [*Holbrook et al.*, 1992], we use the classical definition of seismic lower crust in this paper. The dominant crustal interface C_3 is related to the Conrad discontinuity, and it divides the crust into the upper and lower crust. The upper crust is composed of layers 1, 2 and 3, and the lower crust is composed of layers 4 and 5. Layer 2 is usually a low-velocity zone in the western Sichuan plateau, while it is absent in the Sichuan basin. In the experiment, P_n was observed on two record sections (shot ZIZ and shot LUD-east branch), which are related to the velocity of uppermost mantle of the Sichuan basin. Because of insufficient information about P_n arrival times on the record sections in the western Sichuan plateau, we associate the P_n velocity determined in a study of industrial explosions [*Zhao and Zhang*, 1987] with the layer of uppermost mantle in Figures 12a and 12b.

[43] Layer parameters are given in Table 2; the first quantity is the average layer velocity (km/s), and the second is the average layer thickness (km). A low-velocity zone exists beneath the plateau, but is absent beneath the basin. In the western Sichuan plateau and the Sichuan basin, the average topographic elevation along the profiles is 3874 m and 544 m (see Figure 11), and Moho is at depth of 58 km and 42 km below sea level, so the average crustal thickness is ~62 km and ~43 km, respectively. In the region between Kangding and HYA, the crustal thickness decreases sharply from 63 km to 43 km. The velocity structure at Kangding on line AA' is consistent with that in the northern portion of the Lazha-Changheba profile (Figure 3), i.e., the crustal thickness shows no significant difference (about 61 km), and

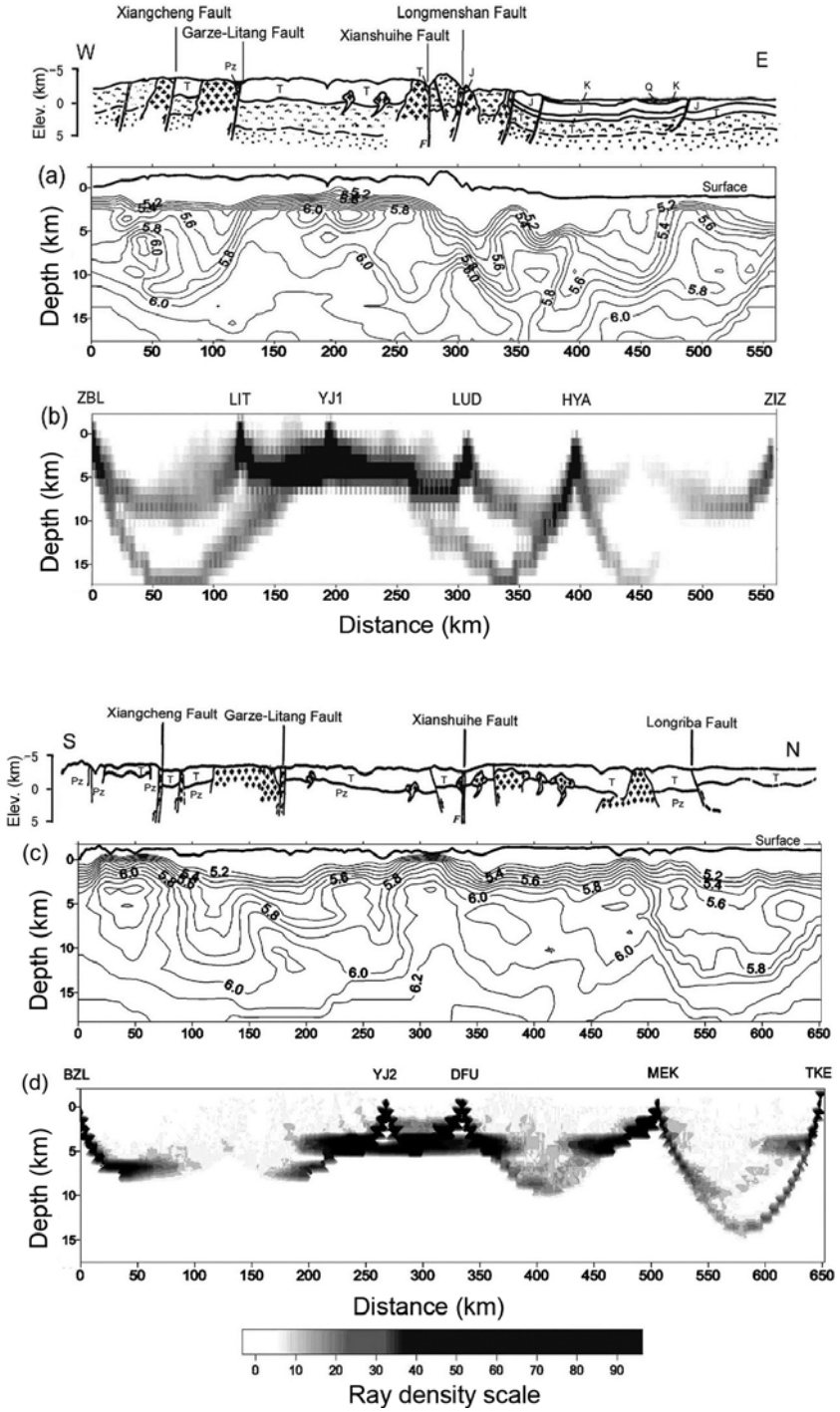

Figure 11. Velocity structure of upper crust with isolines (km/s), derived from finite difference traveltime inversion. Pz, Paleozoic; T, Triassic; J, Jurassic; K, Cretaceous; Q, Quaternary. (a) Geological setting and 2-D velocity structure along line AA'. The Sichuan basin has sediments of about 6 km thickness. (b) P_g ray density along line AA'. (c) Geological setting and 2-D velocity structure along line BB'. The shallow velocity at 40 km north of BZL reaches a maximum of 6.20 km/s. (d) P_g ray density along line BB'. Reference elevation is 3000 m. Ray number is indicated by grey scale.

there exists a low-velocity layer in the upper crust and a low-velocity anomaly in the uppermost mantle along both profiles [*Cui et al.*, 1987]. The crustal structure in the eastern portion of line AA' is similar to the profiles in eastern Yunnan [*Kan et al.*, 1986], which is in the southwestern Yangtze craton.

[44] Along line BB', the average velocity of layer i (i = 1, 2,..., 5) is 6.00, 5.85, 6.18, 6.50, and 6.80 km/s,

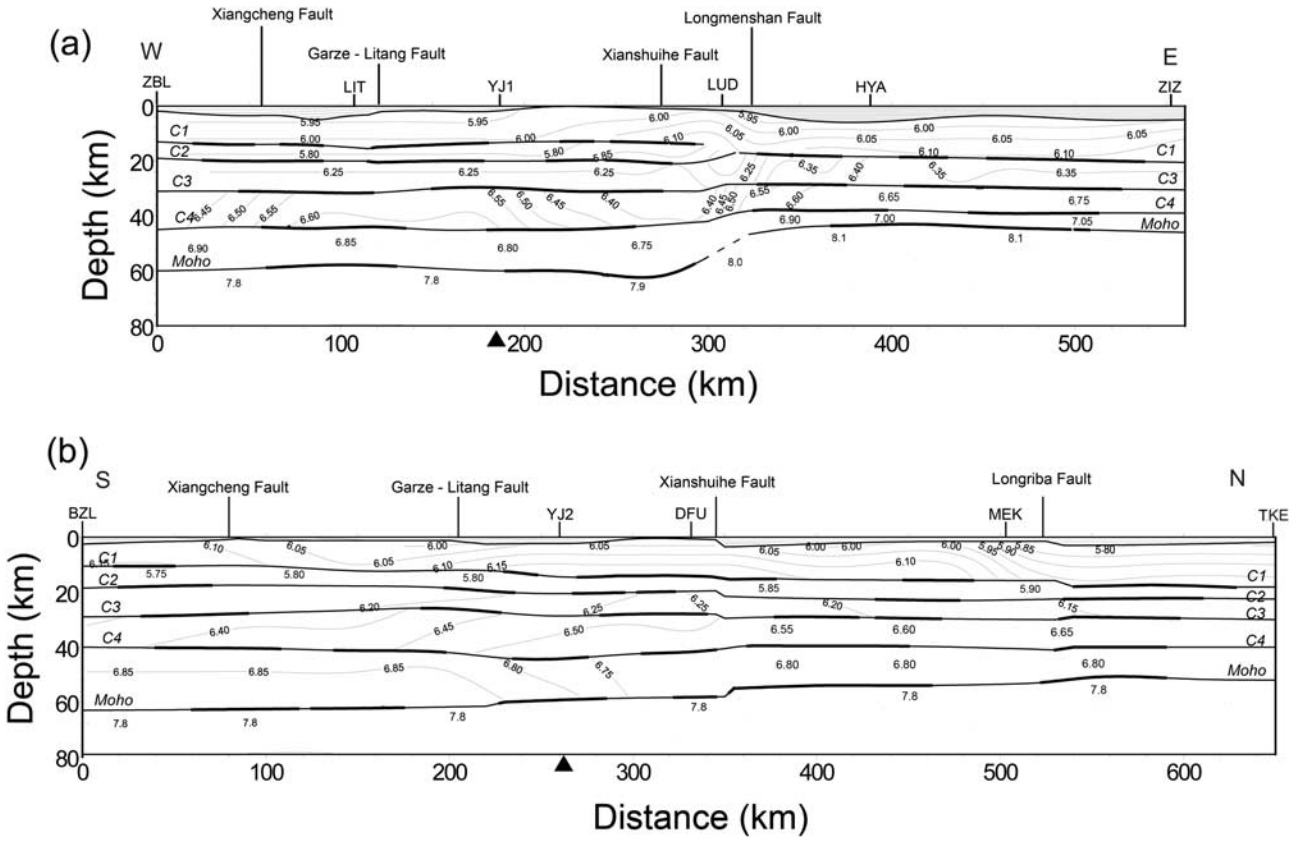

Figure 12. Final 2-D crustal velocity models (km/s). (a) Line AA' and (b) line BB'. Reference elevation is 3000 m. The velocity of the upper crust (0–7 km) is determined from the traveltimes of P_g using finite difference inversion. The bold lines denote reflection regions for phases P_i (i = 1, 2, 3, 4) and P_mP. The corresponding interfaces are labeled as C_i and Moho. Model in Figure 12a shows crustal thinning from the western Sichuan plateau to the Sichuan basin. Model in Figure 12b shows the crust thickening gradually from north to south in the western Sichuan plateau. In the region of shots YJ1 and YJ2 (solid triangle), where the profiles intersect, the crustal velocities along line AA' and line BB' are consistent.

respectively. The crustal thickness gradually increases from 52 km at the northern end, which is close to the crustal thickness of 53 km at Tangke determined by the Longmenshan DSS profile [*Chen et al.*, 1986], to 63 km at the southern end, which is similar to the crustal thickness of 58 km at the northern end of the Simao-Zhongdian DSS profile in the northwestern Yunnan province [*Lin et al.*, 1993]. A seismic reflection profile (named as Hezuo-Tangke profile near the shot point TKE on line BB', see Figure 3) conducted in 2005 for hydrocarbon exploration in the northern Songpan-Garze terrane indicates a crustal thickness of ~51 km [*Gao et al.*, 2005], which is consistent with that in the northern portion of our line BB'. The velocity of layer 1 increases to 6.15 km/s at the southern end which we consider further during our discussion of gravity models (below). In the region of YJ1 and YJ2, where lines AA' and BB' overlap, the crustal structures of the two profiles are very similar, with the only difference being the velocities of layer 1 (Figures 12a and 12b).

[45] Direct indications of a low-velocity layer come from the termination of the Pg phase at a specific offset distance, and the time delay of the wide-angle reflection from the bottom of that layer. This phenomenon is observed on record sections from shots ZBL, LIT and YJ1 (the western branch) (Figures 4 and 5). Another indication of a low-velocity layer from these sections comes from the observation that the phases P_1 and P_2 have similar mean velocity [*Braile and Smith*, 1975]. The amplitudes of seismic phases

Table 2. Comparison of Seismic Velocity in the Western Sichuan Plateau and Sichuan Basin

Geologic Unit	Layer Parameters in Crust: P Velocity, km/s; Thickness, km					Pn Velocity, km/s	Crustal Velocity, km/s	Crustal Thickness, km
	1	2	3	4	5			
Western Sichuan Plateau	5.95; 13	5.85; 9	6.25; 8	6.55; 14	6.80; 17	7.80	6.27	62
Sichuan Basin	6.05; 17	A[a]	6.35; 11	6.75; 11	7.00; 6	8.15	6.45	43

[a]A denotes that layer 2 (low-velocity layer) in the Sichuan basin is absent.

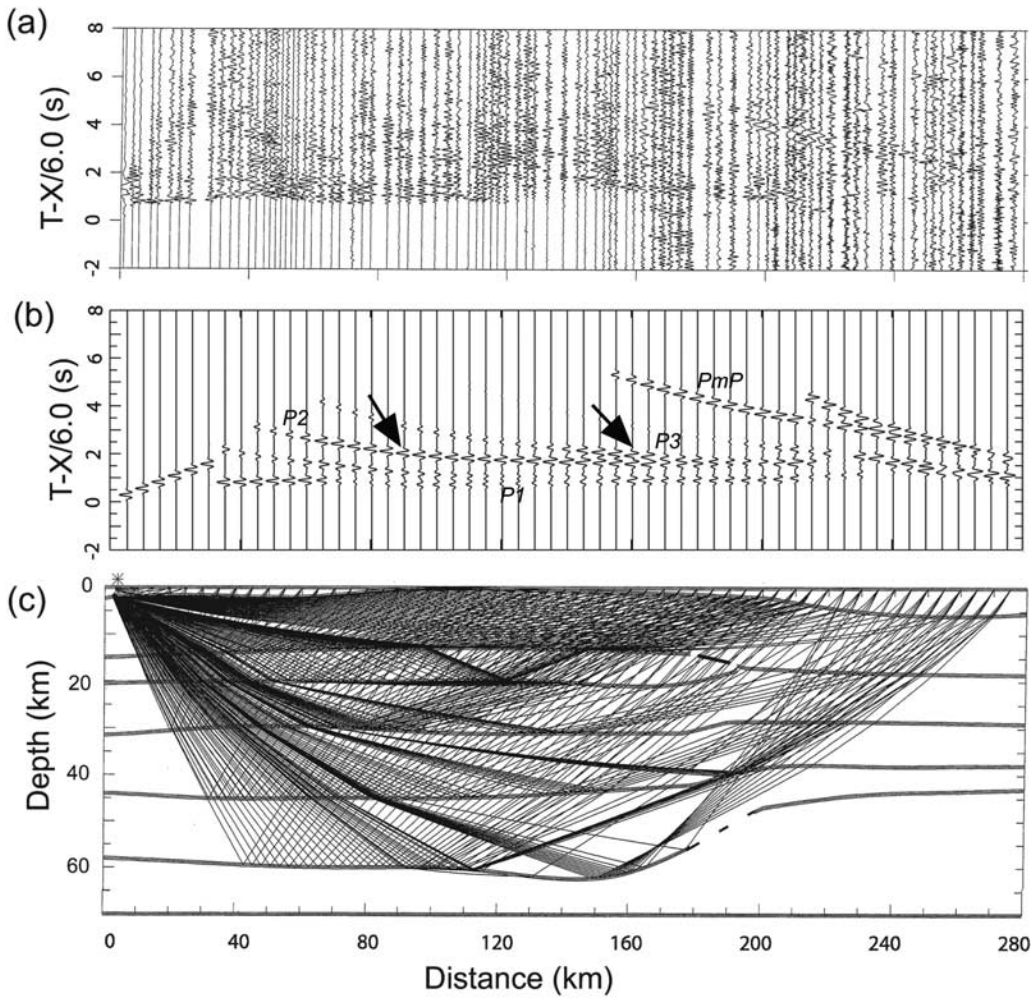

Figure 13. Record section of shot LIT (the eastern branch) along line AA' and interpretation using 2-D ray tracing and synthetic seismograms, based on the 2-D crustal structure in Figure 12a. (a) Trace-normalized record section; (b) trace-normalized synthetic seismograms; (c) raypaths, where an asterisk denotes the shot point. Arrows mark the phases (P_2 and P_3) whose amplitudes are well simulated.

were also modeled to test the hypothesis of a low-velocity layer in the western Sichuan plateau. On the record sections of the shots in the western Sichuan plateau, such as ZBL, LIT, YJ1 (the western branch) and LUD (the western branch) on line AA', and BZL and DFU on line BB', phase P_2 with relatively larger amplitude is interpreted as a reflection from the bottom of a low-velocity layer in the upper crust.

[46] A set of bold lines on each interface in the models along line AA' and line BB', shown in Figures 12a and 12b, implies that the velocity structures are determined by dense ray coverage (see Figures 13c, 14c, and 4–10). The thickness from the reference elevation of 3000 m to the Moho in the western Sichuan plateau was jointly determined from the arrival times of the phase P_mP of several shots, such as LIT, YJ1, DFU, MEK, and TKE, although identification of the phase P_mP in the plateau has higher uncertainty than in the basin. Uncertainty in the final 2-D velocity structures depends upon the shot interval, the recorder interval, and the correct identification of crustal phases. In this study, a layer velocity is primarily determined from an apparent velocity of a refraction phase or the mean velocity determined from a reflection phase. Our estimates of seismic velocity are accurate to around 2% in the upper crust and 3% in the lower crust. The depths of deeper interfaces (e.g., the Moho discontinuity) are accurate to better than 5% of the calculated depth. For instance, an interface at a depth of 60 km could possibly range between 57 km to 63 km. Our assessment of uncertainty in the model velocity structure is comparable to that of *Mooney and Braile* [1989] and *Holbrook et al.* [1992]. The shot point spacing along line AA' is less than that along line BB', so the 2-D velocity structure along line AA' has higher reliability than along line BB', although the recorder interval is similar on both profiles.

[47] Two particular seismic phases were not included in the construction of 2-D velocity structures, because the ray method that we used here is unable to interpret them. One exception is phase P_a on the record section of shot LUD (the western branch), where the phase with low frequency of 1.0 to 1.5 Hz and high apparent velocity of 13.0 to 15.0 km/s appears beyond 160 km (Figure 6a). The phase P_a is probably caused by a local anomaly with high attenuation. Another exception is phase P_b identified on

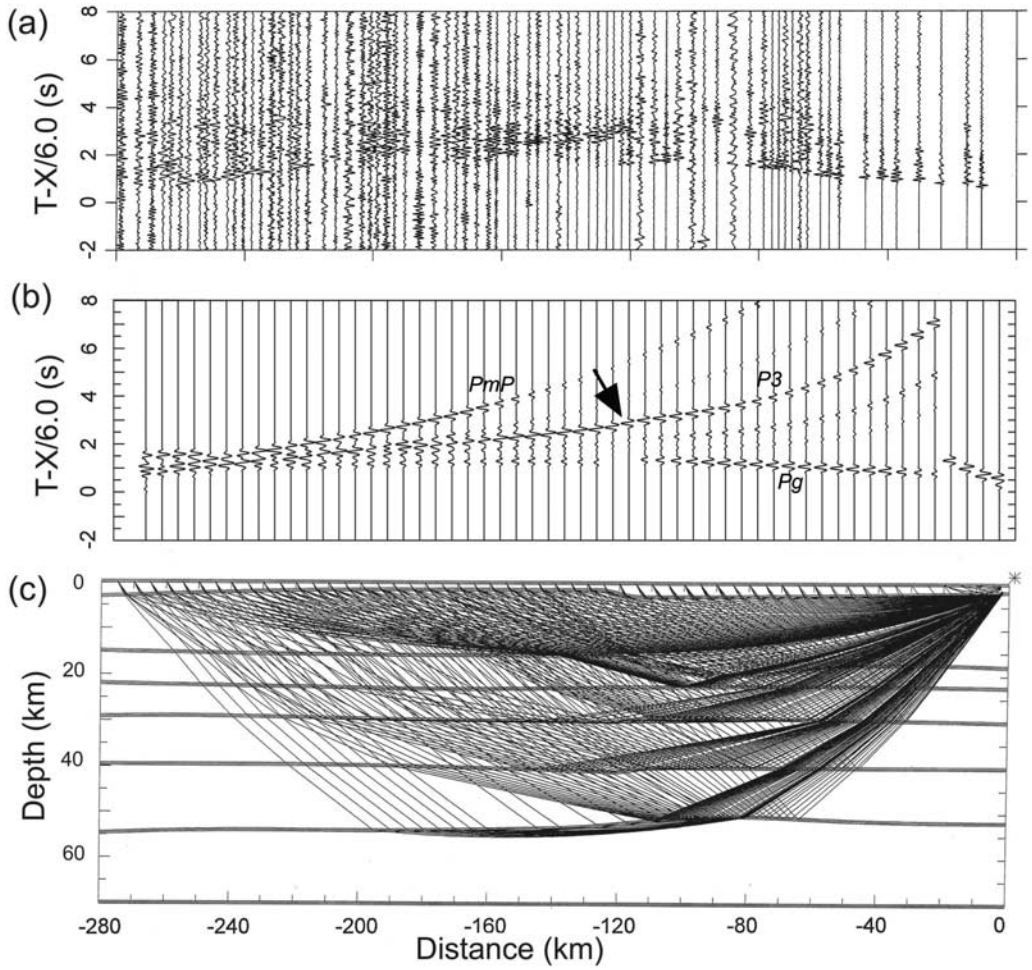

Figure 14. Record section of shot TKE along line BB' and interpretation using 2-D ray tracing and synthetic seismograms, based on the 2-D crustal structure in Figure 12b. (a) Trace-normalized record section; (b) Trace-normalized synthetic seismograms; (c) raypaths, where an asterisk denotes the shot point. Arrows mark the phases (P_3) whose amplitudes are well simulated.

the record section of shot MEK (southern branch); it has frequency components that are typical for a crustal phase (4–6 Hz) but has very low apparent velocity (5.20 km/s) and appears at offsets of 125 to 170 km (Figure 9a). Phase P_b is probably a reflection from an inclined interface, or is a guided wave from a low-velocity channel.

[48] We used ray tracing and synthetic seismograms to compare the fit of our 2-D models to our observations (Figures 13 and 14). A total of 939 arrival times of all phases (P_g, P_1, . . ., P_mP, and P_n) on line AA', and 768 on line BB' were used to determine the respective 2-D crustal structures. The RMS traveltime residuals, which quantify the fit of the final 2-D models, are 0.21 s on line AA' and 0.24 s on line BB'.

4.3. The 2-D Crustal Density Structure

[49] We used the Bouguer gravity data set of China [*Yuan*, 1996], which has typical standard errors in western China of about 3.0 mGal. The eastern margin of the Tibetan Plateau is characterized by a negative Bouguer gravity anomaly (Figure 3). Bouguer gravity anomalies along line AA' (Figure 15a) range from −460 to −140 mGal; the anomaly rapidly increases from −400 mGal at YJ1 to −260 mGal at HYA. Bouguer gravity anomalies along line BB' (Figure 15c) gradually vary from −430 to −360 mGal.

[50] On the basis of the crustal velocity structures derived from the DSS profiles, we constructed initial crustal density models using an empirical velocity-density relation, the Nafe-Drake curve [*Ludwig et al.*, 1970; *Brocher*, 2005], which provides an average fit between density and P velocity. The initial models were refined by performing a forward modeling of the Bouguer gravity data [*Cady*, 1980]. As indicated by the results of our finite difference inversion for the seismic velocity structure, the thickness of the sedimentary layer along line AA' and line BB' varies significantly: sediments in the Sichuan basin are about 6 km thick. The sedimentary layer is assigned a density of 2490 kg/m^3. Figures 15b and 15d show the crustal density structures on lines AA' and BB', respectively, which were determined from the gravity anomalies in Figures 15a and 15c. In general, slight lateral variation of density in each layer exists in the 2-D density models. On the basis of average density of each layer shown in Figure 15, lateral variation of density over a layer falls into the region of ±30 kg/m^3, which is not delineated in the density models. It corresponds to the P velocity lateral variation of 0.15 to

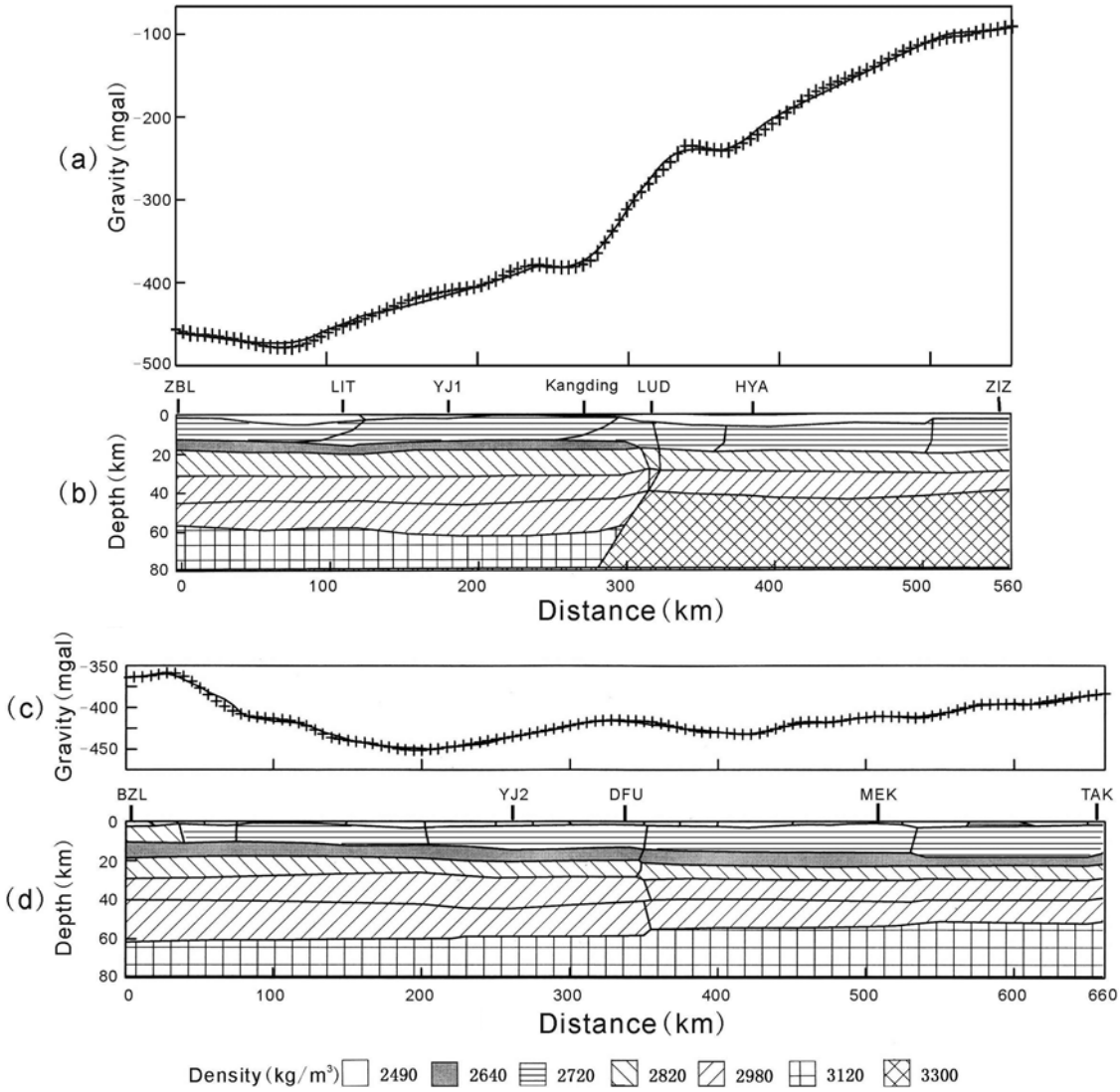

Figure 15. Two-dimensional crustal density models along line AA' and line BB'. (a) Bouguer gravity anomalies (solid line) and calculated anomalies (crosses) along line AA', ranging from −460 to −140 mGal. (b) Crustal density model along line AA' showing rapid crustal thickening from HYA in the Sichuan basin to Kangding in the western Sichuan plateau, and the east and west portions having different density in uppermost mantle. (c) Bouguer gravity anomalies (solid line) and calculated anomalies (crosses) on line BB', ranging from −430 to −360 mGal. (d) Crustal density model along line BB' showing the crust gently thinning from south to north, and high density (2820 and 2980 kg/m^3) in shallow layer above depth of 10 km in upper crust at the southern end of the profile. The density structure at YJ1 in Figure 15b is identical with that at YJ2 in Figure 15d. There is slightly lateral variation (see the main text) of density in each layer of the models. The density shown is an average density over the layer. Reference elevation is 3000 m.

0.20 km/s in a layer of the 2-D velocity models (Figure 12). The RMS fit of the calculated gravity anomalies to the observed anomalies is 2.0 mGal along line AA' and 1.6 mGal along line BB'.

[51] Figure 15b shows that the crustal density cross section of line AA' extends from the western Sichuan plateau to the Sichuan basin, where there is a rapid crustal thickening from HYA in the basin to Kangding in the plateau. In addition, the eastern and western portions of line AA' have different densities in the uppermost mantle of 3300 and 3120 kg/m^3, respectively.

[52] Figure 15d shows that the crustal density cross section along line BB' extends with NNE trend in the Songpan-Garze terrane. At the southern end of line BB' (Figure 15d), our gravity model requires high density (2980 kg/m^3) at shallow depths of <10 km to fit the relatively short wavelength positive gravity anomaly (the most positive gravity values are c. −360 mGal). The region of inferred high density corresponds to a region with high *P* wave velocities (Figure 11), but we note that the velocity-density relation in this region is inconsistent with the Nafe-Drake curve [*Ludwig et al.*, 1970]. The density structures of

both profiles are identical in the region of shot points YJ1 and YJ2, where line AA' intersects with line BB'.

5. Discussion

5.1. Crustal Thickening and Shortening in the Western Sichuan Plateau

[53] There are obvious differences between the western Sichuan plateau and the Sichuan basin in crustal thickness, average crustal velocity, and uppermost mantle (P_n) velocity. In addition, there exists a low-velocity layer in the upper crust of the plateau, whereas the crustal velocity consistently increases with depth in the basin. According to a compilation of global *P* wave velocities [*Holbrook et al.*, 1992], the western Sichuan plateau and the Sichuan basin are characterized as a continental collision zone and a platform, respectively. The Sichuan basin is an old, intact craton that has remained relatively stable despite orogenic events at its margins in the Mesozoic and Cenozoic time [*Burchfiel et al.*, 1995; *Clark and Royden*, 2000]. The crust beneath the basin has higher average *P* wave velocity and has been more rigid than the plateau [*Kohlstedt et al.*, 1995]. During Late Triassic to Early Jurassic time, the collision between rocks in the plateau and rocks in the basin led the plateau to experience strong deformation. As a result, a set of thrust fault zones in the upper crust were generated [*Xu et al.*, 1992] and the crust was thickened. The present deformational field and high elevation of the western Sichuan plateau was established since late Miocene time [*Kirby et al.*, 2002, 2003]. The crust was thickened once more and adjusted isostatically. Consequently, we suggest that the crustal thickness determined in this paper is an accumulated result of crustal thickening in the Late Triassic to Early Jurassic and late Cenozoic. Rock uplift across the eastern margin of the Tibetan Plateau may be a combined isostatic and dynamic response to flow in the lower crust [*Kirby et al.*, 2003]. The crustal variation in thickness and velocity structure along line AA' may be related to the Xianshuihe left lateral fault, with displacement of about 60 km [*Burchfiel et al.*, 1995].

[54] In this study, the traveltimes and apparent (or mean) velocities of P_g to P_3 are related to the velocity structure of the upper crust, whereas those of P_4 and P_mP are related mainly to the lower crust. Comparing the differences from P_g to P_3 between the plateau and the basin, the differences from P_3 to P_mP between the plateau and the basin are shown to be more significant. The records from stations 750 to 794 shown in Figures 16a and 16b, taken from the record sections of shot LIT (Figure 5b) and shot ZIZ (Figure 7), respectively, indicate that the arrival time of P_mP at distance of 210 km for shot LIT is about 3.0 s later than that for shot ZIZ. As a result, the average depth of C_3 is 30 and 28 km and the average thickness of the lower crust (i.e., between C_3 and the Moho) is 31 and 17 km in the crustal models of the plateau and the basin, respectively. Consequently, as shown in Figure 12a, the crustal thickening along the profile is inferred to be mainly in the lower crust.

[55] A magnetotelluric survey along line AA' [*Sun et al.* 2003] reveals a low-resistivity (several to tens of ohm m) layer in the upper crust of the western Sichuan plateau at a similar depth to the low-velocity layer that we detect. The coincidence of low resistivity and low velocity may be caused by overpressured hydrous fluids or melt [*Keller*, 1989; *Jones*, 1992]. Partial melt or aqueous fluids in midcrust in the Himalaya and southern Tibet have been inferred from magnetotelluric data [*Li et al.*, 2003; *Wei et al.*, 2001; *Spratt et al.*, 2005] and wide-angle seismic data [*Makovsky and Klemperer*, 1999]. The inference of overpressured hydrous fluid or melt suggests that the zone is weak and is actively deforming [*Klemperer*, 2006]. High heat flow and exposed fault rocks that are interpreted as an exhumed ductile detachment [*Hu et al.*, 2000; *Xu et al.*, 1992] lead us to suggest that the low-resistivity and low-velocity zone beneath the western Sichuan plateau is an active ductile detachment within relatively hot crust. We propose that a set of west dipping upper crustal thrust faults mapped along the central western portion of line AA' might have listric shape and detach within this zone.

5.2. Weak Energy of the Phase *PmP* Within the Western Sichuan Plateau

[56] The amplitude of the seismic signal recorded at a station is related to local site conditions, anelastic medium attenuation, scattering, and the size of the source input signal. Because of a general lack of information regarding site conditions at the DSS temporary stations during the field experiment, the absolute amplitude of each phase could not be precisely observed. Instead, relative amplitude between two phases on the same record, or between two records at the same station from different shots, can be used to achieve useful information about the medium attenuation. The seismic phase P_mP on the record sections (e.g., Figures 4, 5b, 6a, and 10) in the western Sichuan plateau is generally weak. To understand the amplitude variation of phase P_mP along line AA', seismic records were analyzed in the following manner:

5.2.1. Comparison of Records in Reverse Branches From Shot LUD

[57] On the record sections of shot LUD, P_mP arrival is not clear in the western branch (Figure 6a), but it is fairly distinct in the eastern branch (Figure 6b). We suggest that this is because the amplitude of the P_mP arrival in the western branch is much less than that in the eastern branch. The P_mP western branch was recorded in the western Sichuan plateau, while P_mP in the eastern branch is mainly related to the velocity structure in the lower crust of the Sichuan basin (see Figure 16d). The amplitude of P_mP in the western branch did not reduce by station/recorder coupling. The record sections of shots BZL, LIT and YJ1 (Figures 4 and 5b) show there is better station/recorder coupling at stations west of shot LUD, though we do not know the exact station/record coupling.

5.2.2. Comparison of Records From Shots LIT and ZIZ at the Same Stations

[58] Figure 16c is plotted using the same amplitude scale as Figure 16b on the basis of the average background noise level in the data from -2 s to -1 s of the reduced time on the record sections. We did not take account of the possible effects of shot energy coupling in this study. Besides having nearly the same shot-station distances from shots LIT and ZIZ, the location and instrumental parameters at the same station are of course identical for both shots. Figures 16b and 16c show that the amplitude of phase P_mP from the 2500-kg shot ZIZ is much larger than from the 3000-kg shot

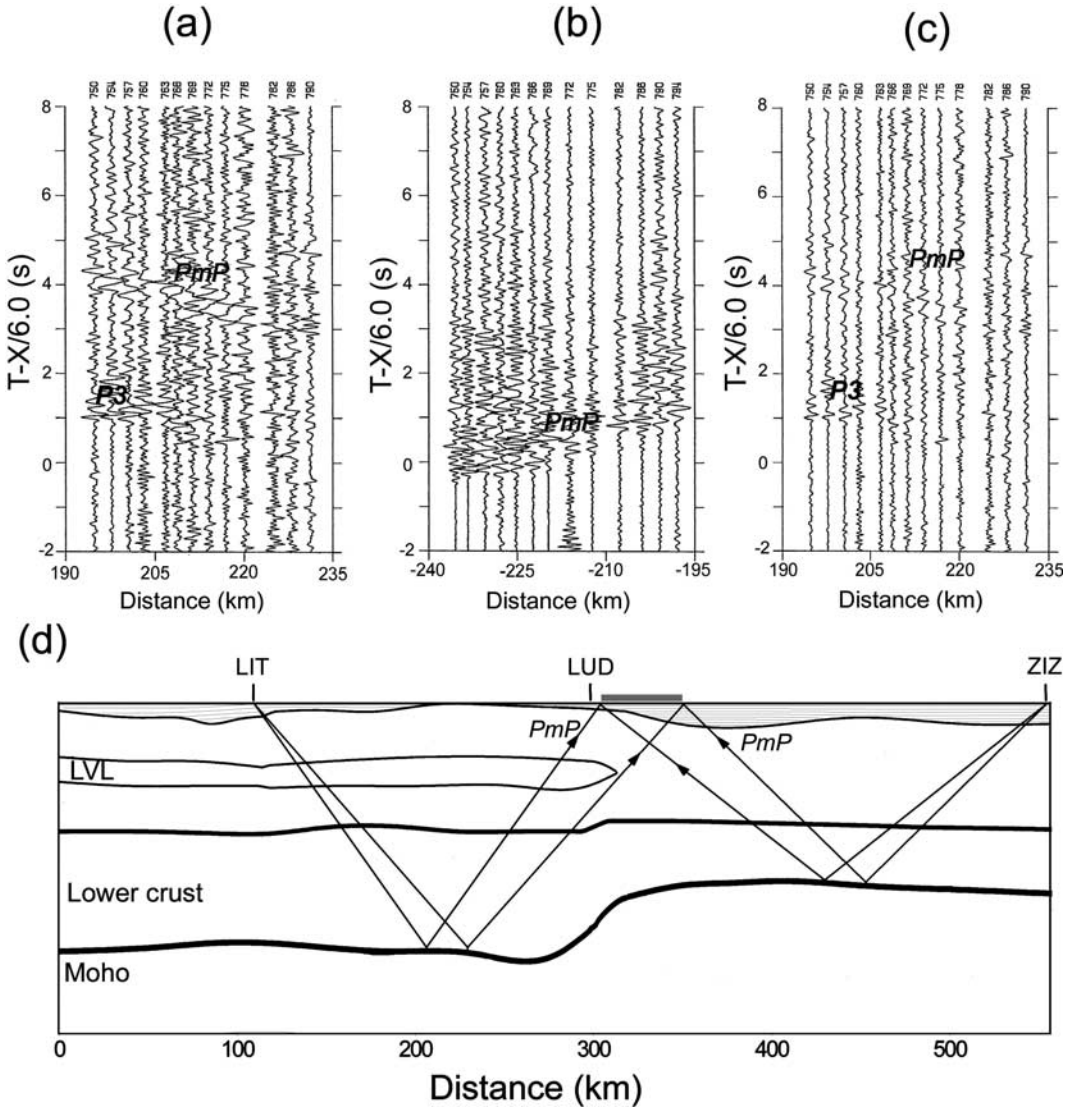

Figure 16. Record sections from stations numbered 750 to 794 along line AA'. (a) shot LIT; (b) shot ZIZ; (c) shot LIT; and (d) sketch map of the station locations and P_mP raypaths from shots to stations. The station number is marked at the top of each record trace. The station with same number on the record sections has same location and instrumental parameters. Grey area in Figure 16d indicates the station location. The station groups in Figures 16a, 16b, and 16c have nearly the same shot-station distance from shot LIT and shot ZIZ along line AA'. The record sections in Figures 16a and 16b are plotted using normalized trace and low-pass filter (8 Hz). The record sections in Figures 16a and 16c have a different amplitude scale, and Figure 16c is plotted using the same amplitude scale as the record section in Figure 16b on the basis of the average background noise level.

LIT. There is not only a variation in amplitude characteristics, but also even more pronounced, a variation in traveltime and mean velocity, indicating different crustal thicknesses. The stations numbered 750 to 794 are located east of shot LUD (Figure 16d), so the relative amplitude variation of phase P_mP from shot LIT and shot ZIZ indicates different characteristics of crustal attenuation between the plateau and the basin.

[59] Under the assumption of an elastic medium, the synthetic seismograms predict that the P_mP amplitude observed in the Sichuan basin is obviously larger than that observed in the western Sichuan plateau (e.g., Figures 13 and 14). It could be caused by either a smaller velocity contrast at the crust-mantle transition, as the results of magmatic underplating on the reflection interface, or by anomalous anelastic properties within the medium above the Moho. A broadband teleseismic observation profile conducted in 2004–2006 coincides with the E–W trending DSS profile of this study. Receiver functions at stations along the profile show strong P to S converted phases from the Moho [*Wang et al.*, 2006], indicative of a sharp discontinuity. In addition, the Hezuo-Tangke deep seismic reflection profile in northern Songpan-Garze terrane shows clear Moho reflections [*Gao et al.*, 2005]. We explore the hypothesis that medium anelasticity leads to an anomalously weak P_mP phase and propose the presence of a medium

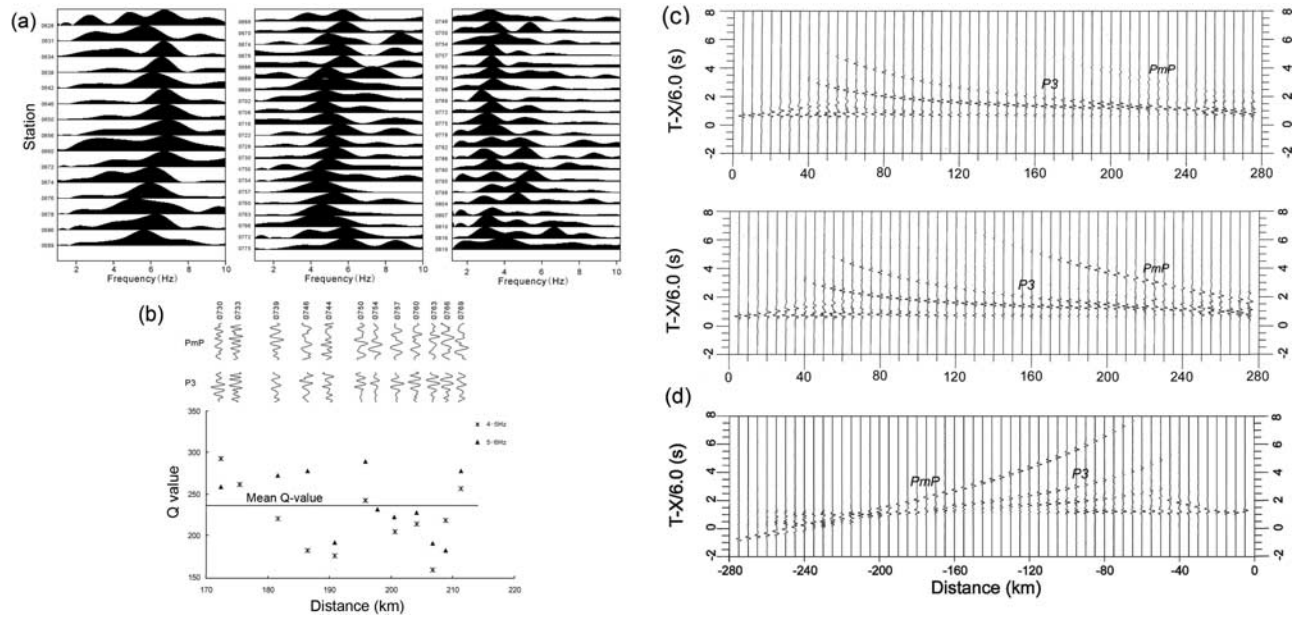

Figure 17. Estimate of Q_p for the lower crust and synthetic seismograms. (a) Amplitude spectra of phases (left) P_1, (middle) P_3, and (right) P_mP on the records (with station number) of shot LIT (the eastern branch). (b) Estimated Q_p of the lower crust at stations. (top) Record segments of phases P_mP and P_3; (bottom) Q_p values at 4–5 Hz and 5–6 Hz, and the average Q_p value. (c) Trace-normalized synthetic seismograms for shot LIT with Q_p = 100 and 300 in lower crust. The 1-D velocity model is defined as the layered homogeneous medium from surface to depth: (thickness, km; P velocity km/s) = (2.0, 4.9); (10.0, 6.03); (8.0, 5.85); (11.0, 6.25); (13.0, 6.50); (16.0, 6.75); (∞, 7.80). (top) Synthetic seismograms with Q_p = 100 in lower crust; (bottom) synthetic seismograms with Q_p = 300 in lower crust. Trace-normalized record section of shot LIT (the eastern branch) is shown in Figure 5b. (d) Trace-normalized synthetic seismograms for shot ZIZ with Q_p = 1000 in lower crust. The 1-D velocity model is defined as (thickness km; P velocity, km/s) = (4.0, 4.90); (16.0, 6.15); (10.0, 6.40); (11.0, 6.85); (6.0, 7.10); (∞, 8.15). Trace-normalized record section of shot ZIZ is shown in Figure 7.

with high attenuation (low Q_p) in the lower crust beneath the western Sichuan plateau.

[60] We apply the spectral ratio method [*Teng*, 1968] to the records of shot LIT (the eastern branch) to estimate Q_p of lower crust beneath the western Sichuan plateau. Spectral analysis of the records shows that the spectral peak ranges from 4 Hz to 6 Hz for phase P_3 and from 2 Hz to 4 Hz for phase P_mP (Figure 17a). We selected 12 records at distances from 170 km to 215 km, where both phases P_3 and P_mP are clear in each record. The amplitude spectral ratio of the phases P_3 and P_mP on the records was used to estimate Q_p in the lower crust, assuming that the upper crust is elastic (see method description in the auxiliary material). On the basis of the amplitude spectra of phases P_3 and P_mP on the 12 records, Q_p of the lower crust was estimated to be 248 ± 40 at frequencies from 4 Hz to 5 Hz and to be 233 ± 42 at frequencies from 5 Hz to 6 Hz, respectively. Our best estimate of Q_p for the lower crust beneath the western Sichuan plateau is 242 ± 41, which is arithmetic mean of all Q_p measurements (Figure 17b).

[61] Previous studies [e.g., *Hwang and Mooney*, 1986; *Benz et al.*, 1990] indicate that lower crustal Q_p values in continents are moderately high (400–1000), although these estimates along the DSS profiles have large error bars. We calculated synthetic seismograms for layered media with different Q_p values by use of the reflectivity method [*Fuchs and Mueller*, 1971; *Sandmeier and Wenzel*, 1986] to fit the record sections in a manner similar to the interpretation by *Hwang and Mooney* [1986] for the Great Valley, California. Figures 17c and 17d show synthetic seismograms of the 1-D model with Q_p values that fit the observed data from shot LIT (the eastern branch) and shot ZIZ (Figures 5b and 7). Taking into account the relative amplitude between P_3 and P_mP, the trace-normalized synthetic seismograms with Q_p = 300 in the lower crust fit the records of shot LIT (Figure 17b), and are consistent with results from the spectral ratio method. The observation that P_mP arrivals from shot LIT (the eastern branch) are clearer than from other shots (see Figures 4, 6a, 8, and 9a) leads us to suggest that Q_p values of the lower crust in the western Sichuan plateau are <300, and the likely range is 100–300 (Figure 17c). In contrast to the western Sichuan plateau, Q_p values of the lower crust in the Sichuan basin are estimated to be 1000 or more (Figure 17d). We suggest that high attenuation in the lower crust beneath the western Sichuan plateau is a consequence of lower crustal flow. Figure 18 illustrates our crustal kinematic model for the eastern margin of the Tibetan Plateau.

6. Conclusions

[62] We present active source seismic refraction and wide-angle reflection data that constrain the crustal structure

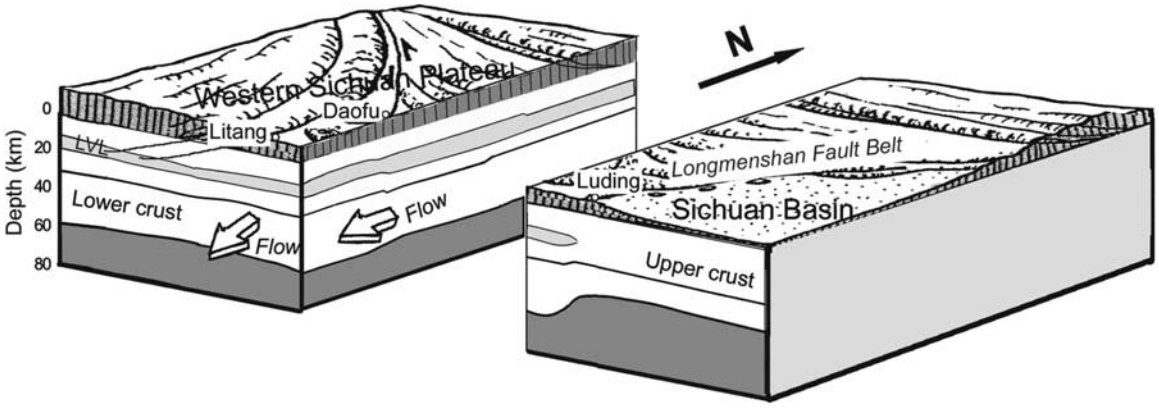

Figure 18. Three-dimensional sketch diagram of our crustal kinematic model for the eastern margin of the Tibetan Plateau, constructed from the 2-D crustal structures of the profiles. Crustal thickening along the DSS profiles occurs mainly in the lower crust. High attenuation (Q_p = 100–300) is used to suggest active lower crustal flow beneath the western Sichuan plateau.

of the eastern margin of the Tibetan Plateau. Density models constructed from the seismic *P* velocity models are consistent with observed Bouguer gravity anomalies. The western Sichuan plateau shows obvious differences from the Sichuan basin in crustal thickness, average crustal velocity and P_n velocity. A low-velocity and low-resistivity layer exists in the upper crust beneath the western Sichuan plateau. The inferred crustal structures are related to the tectonics of the eastern margin of the Tibetan Plateau, which experienced deformation phases during the Late Triassic to Early Jurassic and the late Cenozoic [*Kirby et al.*, 2002, 2003]. The low-velocity and low-resistivity layers may be reactivated structures that play a role in the process of detachment and thrust shear, associated with upper crustal shortening, though the present-day rates of shortening are probably <3 mm/yr [*Burchfiel et al.*, 1995; *Chen et al.*, 2000]. We infer from our observations that crustal thickening, and presumably uplift of the western Sichuan plateau is a result of lower crustal thickening. The present crustal thickness is a combined result of crustal thickening during the Mesozoic and late Cenozoic. We observed high attenuation (Q_p = 100–300) in the lower crust of the western Sichuan plateau and propose this as supporting evidence for active flow of an overthickened crust.

[63] **Acknowledgments.** This research was conducted with support from the Continental Dynamics program of the State Natural Scientific Foundation of China (grant 40334041) and the International Cooperation Program of the Department of Science and Technology of China (grant 2003DF000011). The fieldwork was supported by the State Key Basic Research Development and Programming Project of China (grant G1998040700/95-13-02-03). The authors sincerely appreciate the help and fieldwork assistance received from the Geophysical Exploration Center, China Seismological Bureau and from the Sichuan Seismological Bureau of China. The authors are most grateful to R. Sutherland, P. Molnar, E. Lüeschen, I. Manighetti, L. Zhu, and Anonymous for their contributions in the improvement of this manuscript. We dedicate this paper to Li Ping and Zhang Xin-Zhong, who perished while conducting fieldwork for this study in the Tibetan Plateau.

References

Allen, C. R., Z. L. Lou, H. Qian, X. Z. Wen, H. W. Zhou, and W. S. Huang (1991), Field study of a highly active fault zone: The Xianshuihe fault of southwestern China, *Geol. Soc. Am. Bull.*, *103*, 1178–1199.

Ammon, C. J., and J. E. Vidale (1993), Tomography without rays, *Bull. Seismol. Soc. Am.*, *83*, 509–528.

Barazangi, M., and J. Ni (1982), Velocities and propagation characteristics of P_n and S_n beneath the Himalayan arc and Tibetan Plateau: Possible evidence for underthrusting of Indian continental lithosphere beneath Tibet, *Geology*, *10*, 179–185.

Benz, H. M., R. B. Smith, and W. D. Mooney (1990), Crustal structure of the northwestern Basin and Range Province from the 1986 Program for Array Seismic Studies of the Continental Lithosphere seismic experiment, *J. Geophys. Res.*, *95*, 21,823–21,842.

Bird, P. (1991), Lateral extrusion of lower crust from under high topography, in the isostatic limit, *J. Geophys. Res.*, *96*, 10,275–10,286.

Block, L., and L. H. Royden (1990), Core complex geometries and regional scale flow in the lower crust, *Tectonics*, *9*, 557–567.

Braile, L. W., and R. B. Smith (1975), Guide to the interpretation of crustal refraction profiles, *Geophys. J. R. Astron. Soc.*, *40*, 145–176.

Brocher, T. M. (2005), Empirical relations between elastic wavespeeds and density in the Earth's crust, *Bull. Seismol. Soc. Am.*, *95*, 2081–2092, doi:10.1785/0120050077.

Burchfiel, B. C., Z. Chen, Y. Liu, and L. H. Royden (1995), Tectonics of Longmen Shan and adjacent regions, central China, *Int. Geol. Rev.*, *37*, 661–736.

Cady, J. W. (1980), Calculation of gravity and magnetic anomalies of finite-length right polygonal prisms, *Geophysics*, *45*, 1507–1512.

Cerveny, V., and I. Psencik (1984), SEIS83–numerical modeling of seismic wavefield in 2-D laterally varying layered structures by the ray method, in *Documentation of Earthquake Algorithms*, edited by E. R. Engdahl, *Rep. SE-35*, pp. 36–40, World Data Center (A) for Solid Earth Geophys., Boulder, Colo.

Cerveny, V., I. A. Molotkov, and I. Psencik (1977), *Ray Method in Seismology*, 214 pp., Univ. Karlova, Prague.

Chen, S. F., C. J. L. Wilson, Q. D. Deng, X. L. Zhao, and Z. L. Luo (1994), Active faulting and block movement associated with large earthquakes in the Min Shan and Longmen mountains, northeastern Tibetan Plateau, *J. Geophys. Res.*, *99*, 24,025–24,038.

Chen, W. P., and P. Molnar (1981), Constraints on the seismic wave velocity structure beneath the Tibetan Plateau and their tectonic implication, *J. Geophys. Res.*, *86*, 5837–5963.

Chen, X. B., Y. Q. Wu, P. S. Du, J. S. Li, Y. R. Wu, G. F. Jiang, and J. X. Zhao (1986), Crustal velocity structure at two sides of Longmenshan tectonic belt (in Chinese), in *Developments in the Research of Deep Structure of China's Continent*, pp. 112–127, Dep. of Sci. Program. and Earthquake Monit., China Seismol. Bur., Seismol. Press, Beijing.

Chen, Z., B. C. Burchfiel, Y. Liu, R. W. King, L. H. Royden, W. Tang, E. Wang, J. Zhao, and X. Zhang (2000), Global positioning system measurements from eastern Tibet and their implications for India/Eurasia intercontinental deformation, *J. Geophys. Res.*, *105*, 16,215–16,227.

Clark, M. K., and L. H. Royden (2000), Topographic ooze: Building the eastern margin of Tibet by lower crustal flow, *Geology*, *28*, 703–706.

Conrad, V. (1925), Laufzeitkurven des Tauernbebens vom 28. November 1923, *Mitt. Erdb. Komm. Wiener Akad. Wiss.*, *59*, 1–23.

Cui, Z. Z., D. Y. Lu, and J. P. Chen (1987), Deep crustal structure and tectonics in Panxi region (in Chinese), *Acta Geophys. Sin.*, *30*, 566–580.

Cui, Z. Z., J. P. Chen, and L. Wu (1996), *Deep Crustal Structure and Tectonics in Huashixia-Shaoyang Profile* (in Chinese), pp. 156–168, Geol. Press, Beijing.

England, P. C., and G. A. Houseman (1986), Finite strain calculation of continental deformation: 2. Comparison with the India-Asia collision zone, *J. Geophys. Res.*, *91*, 3664–3676.

Fuchs, K., and G. Mueller (1971), Computation of synthetic seismograms with the reflectivity method and comparison with the observations, *Geophys. J. R. Astron. Soc.*, *23*, 417–433.

Gajewski, D., and C. Prodehl (1987), Seismic refraction investigation of the Black Forest, *Tectonophysics*, *142*, 27–48.

Gao, R., Y. Ma, and X. Zhu (2005), Lithospheric structure of the Songpan block in the northeastern Tibetan Plateau: Revelation from investigation of the deep seismic reflection profile, in *20th Himalayan–Karakoruan–Tibet Workshop Special Extended Abstract*, *Geol. Alpine Mem. H. S.*, vol. 44, edited by G. Mascle and J. Lave, pp. 58–59, Lab. of Geodyn. of the Alpine Chains, Univ. Joseph Fourier-Grenoble 1, Grenoble, France.

Giese, P., and C. Prodehl (1976), Problems of evaluation of seismic refraction data for crustal and upper mantle studies, in *Explosion Seismology in Central Europe: Data and Results*, edited by P. Giese, C. Prodehl, and A. Stein, pp. 148–149, Springer-Verlag, Berlin.

Gu, G. X. (1983), *Catalog of Chinese Earthquakes* (*1831 B.C.–1969 A.D.*) (in Chinese), pp. 200–201, Sci. Press, Beijing.

Hirn, A., J.-C. Lepine, and G. Jobert (1984), Crustal structure and variability for the Himalayan border of Tibet, *Nature*, *307*, 23–25.

Holbrook, W. S., W. D. Mooney, and N. J. Christensen (1992), The seismic velocity structure of the deep continental crust, in *Continental Lower Crust*, edited by D. M. Fountain, R. Arculus, and R. W. Kay, pp. 1–34, Elsevier Sci., Amsterdam.

Hole, J. A. (1992), Nonlinear high-resolution three-dimensional seismic travel time tomography, *J. Geophys. Res.*, *97*, 6553–6562.

Hu, S., L. He, and J. Wang (2000), Heat flow in the continental area of China: A new data set, *Earth Planet. Sci. Lett.*, *179*(2), 407–419.

Huang, J., D. Zhao, and S. Zheng (2002), Lithospheric structure and its relationship to seismic and volcanic activity in southwest China, *J. Geophys. Res.*, *107*(B10), 2255, doi:10.1029/2000JB000137.

Hwang, L., and W. D. Mooney (1986), Velocity and *Q* structure of the Great Valley, California, based on synthetic seismograms modeling of seismic refraction data, *Bull. Seismol. Soc. Am.*, *76*, 1053–1067.

Jeffreys, H. (1926), On compressional waves in two superposed layers, *Proc. Cambridge Philos. Soc.*, *23*, 472–481.

Jones, A. G. (1992), Electrical properties of the continental lower crust, in *Continental Lower Crust*, edited by D. M. Fountain, R. Arculus, and R. W. Kay, pp. 81–143, Elsevier Sci., Amsterdam.

Jones, L. M., W. Han, E. Hauksson, A. Jin, Y. Zhang, and Z. Lou (1984), Focal mechanisms of the Songpan earthquakes of August 1976 in Sichuan, China, *J. Geophys. Res.*, *89*, 7697–7707.

Kan, R., H. Hu, R. Zeng, W. D. Mooney, and T. V. McEvilly (1986), Crustal structure of Yunnan Province, People's Republic of China, from seismic refraction profiles, *Science*, *234*, 433–437.

Keller, G. V. (1989), Electrical structure of the crust and upper mantle beneath the United States, part 1, Methods for determining the conductivity profile, in *Geophysical Framework of the Continental United States*, edited by L. C. Pakiser and W. D. Mooney, *Mem. Geol. Soc. Am.*, *172*, 425–446.

King, R. W., F. Shen, B. C. Burchfiel, L. H. Royden, E. Wang, Z. Chen, Y. Liu, X. Zhang, J. Zhao, and Y. Li (1997), Geodetic measurement of crustal motion in southwest China, *Geology*, *25*, 179–182.

Kirby, E., P. W. Reiners, M. A. Krol, K. X. Whipple, K. V. Hodges, K. A. Farley, W. Tang, and Z. Chen (2002), Late Cenozoic evolution of the eastern margin of the Tibetan Plateau: Inferences from $^{40}Ar/^{39}Ar$ and (U-Th)/He thermochronology, *Tectonics*, *21*(1), 1001, doi:10.1029/2000TC001246.

Kirby, E., K. X. Whipple, W. Tang, and Z. Chen (2003), Distribution of active rock uplift along the eastern margin of the Tibetan Plateau: Inferences from bedrock channel longitudinal profiles, *J. Geophys. Res.*, *108*(B4), 2217, doi:10.1029/2001JB000861.

Klemperer, S. L. (2006), Crustal flow in Tibet: A review of geophysical evidence for the physical state of Tibetan lithosphere, in *Channel Flow, Ductile Extrusion and Exhumation of Lower Mid-Crust in Continental Collision Zones*, edited by M. P. Searle and R. D. Law, *Geol. Soc. Spec. Publ.*, *268*, 39–70.

Kohlstedt, D. L., B. Evans, and S. J. Mackwell (1995), Strength of the lithosphere: Constraints imposed by laboratory experiments, *J. Geophys. Res.*, *100*, 17,587–17,602.

Larson, K. M., R. Burgman, and R. Bilham (1999), Kinematics of the India-Eurasia collision zone from GPS measurements, *J. Geophys. Res.*, *104*, 1077–1093.

Li, P. (1993), *The Xiangshuihe-Xiaojiang Fault Belt* (in Chinese), 50 pp., Seismol. Press, Beijing.

Li, S., M. J. Unsworth, J. R. Booker, W. Wei, H. Tan, and A. G. Jones (2003), Partial melt or aqueous fluid in the mid-crust of southern Tibet? Constraints from INDEPTH magnetotelluric data, *Geophys. J. Int.*, *153*, 289–304.

Lin, Z. Y., H. X. Hu, W. B. Zhang, H. F. Zhang, Z. Q. He, Z. M. Lin, and T. X. Qiu (1993), The preliminary interpretation of deep seismic sounding in western Yunnan (in Chinese), *Acta Seismol. Sin.*, *15*, 427–440.

Liu, J. H., F. T. Liu, H. Wu, Q. Li, and G. Hu (1989), Three dimensional velocity images of the crust and upper mantle beneath north-south zone in China (in Chinese), *Acta Geophys. Sin.*, *32*, 143–152.

Ludwig, W. J., J. E. Nafe, and C. L. Drake (1970), Seismic refraction, in *The Sea*, vol. 4, edited by A. E. Maxwell, pp. 53–84, Wiley-Interscience, New York.

Lutter, W. J., G. S. Fuis, C. H. Thurber, and J. Murphy (1999), Tomographic images of the upper crust from the Los Angeles basin to the Mojave Desert, California: Results from the Los Angeles Region Seismic Experiment, *J. Geophys. Res.*, *104*, 25,543–25,565.

Makovsky, Y., and S. L. Klemperer (1999), Measuring the seismic properties of Tibetan bright spots: Evidence for free aqueous fluids in the Tibetan middle crust, *J. Geophys. Res.*, *104*, 10,795–10,825.

Meissner, R. (1986), *The Continental Crust: A Geophysical Approach*, 426 pp., Academic, London.

Molnar, P., and W.-P. Chen (1978), Evidence for large Cenozoic crustal shortening of Asia, *Nature*, *273*, 218–220.

Molnar, P., and P. Tapponnier (1975), Tectonics in Asia: Consequences and implications of a continental collision, *Science*, *189*, 419–426.

Mooney, W. D. (1989), Seismic methods for determining earthquake source parameters and lithospheric structure, in *Geophysical Framework of the Continental United States*, edited by L. C. Pakiser and W. D. Mooney, *Mem. Geol. Soc. Am.*, *172*, 11–34.

Mooney, W. D., and L. W. Braile (1989), The seismic structure of the continental crust and upper mantle of North America, in *The Geology of North America: An Overview*, edited by A. W. Bally and A. R. Palmer, pp. 39–52, Geol. Soc. of Am., Boulder, Colo.

Nelson, K. D., et al. (1996), Partially molten middle crust beneath southern Tibet: Synthesis of project INDEPTH results, *Science*, *274*, 1684–1688.

Ni, J., and M. Barazangi (1984), Seismotectonics of the Himalayan collision zone: Geometry of underthrusting Indian plate beneath the Himalaya, *J. Geophys. Res.*, *89*, 1147–1164.

Owens, T. J., and G. Zandt (1997), Implications of crustal property variations for model of Tibetan Plateau evolution, *Nature*, *387*, 37–43.

Papadimitriou, E., X. Wen, V. Karakostas, and X. Jin (2004), Earthquake triggering along the Xianshuihe fault zone of western Sichuan, China, *Pure Appl. Geophys.*, *161*, 1683–1707.

Parsons, T., J. McCarthy, W. M. Kohler, C. J. Ammon, H. M. Benz, J. A. Hole, and E. E. Criley (1996), Crustal structure of the Colorado Plateau, Arizona: Application of new long-offset seismic data analysis techniques, *J. Geophys. Res.*, *101*, 11,173–11,194.

Ren, J. X., Z. X. Wang, and B. W. Chen (1999), *Tectonic Maps of China and Its Surrounding Region* (in Chinese), Geol. Press, Beijing.

Royden, L. H., B. C. Burchfiel, R. W. King, E. Wang, Z. Chen, F. Shen, and Y. Liu (1997), Surface deformation and lower crustal flow in eastern Tibet, *Science*, *276*, 788–790.

Sandmeier, K.-J., and F. Wenzel (1986), Synthetic seismograms for a complex crustal model, *Geophys. Res. Lett.*, *13*, 22–25.

Sheriff, R. E., and L. P. Geldart (1995), *Exploration Seismology*, 592 pp., Cambridge Univ. Press, New York.

Sichuan Seismological Bureau (1989), *Xianshuihe Active Fault Belt* (in Chinese), Sichuan Sci. and Technol. Press, Chengdu, China.

Spratt, J. E., A. G. Jones, K. D. Nelson, M. J. Unsworth, and INDEPTH MT Team (2005), Crustal structure of the India-Asia collision zone, southern Tibet, from INDEPTH MT investigations, *Phys. Earth Planet. Inter.*, *150*, 227–237.

Sun, J., G. W. Jin, and D. H. Bai (2003), Exploration of the electrical structure in the crust and upper mantle in eastern margin of Tibetan Plateau and its geotectonic implications, *Sci. China, Ser. D*, *46* (Suppl.), 243–253.

Sun, R. M., F. T. Liu, and J. H. Liu (1991), Seismic tomography of Sichuan region (in Chinese), *Acta Geophys. Sin.*, *34*, 708–716.

Tapponnier, P., G. Peltzer, A. Y. Le Dain, R. Armijo, and P. Cobbold (1982), Propagating extrusion tectonics in Asia: New insight from simple experiments with plasticine, *Geology*, *10*, 611–616.

Teng, J. W. (1994), *Lithospheric Physics and Dynamics in Kang-Dian Tectonic Zone, China* (in Chinese), pp. 102–121, Sci. Press, Beijing.

Teng, T. L. (1968), Attenuation of body waves and the *Q* structure of the mantle, *J. Geophys. Res.*, *73*, 2195–2208.

Vidale, J. E. (1988), Finite-difference traveltime calculation, *Bull. Seismol. Soc. Am.*, *78*, 2062–2076.

Wang, C.-Y., R. S. Zeng, W. D. Mooney, and B. R. Hacker (2000), A crustal model of the ultrahigh-pressure Dabie Shan orogenic belt, China, derived from deep seismic-refraction profiling, *J. Geophys. Res.*, *105*, 10,857–10,869.

Wang, C., W. W. Chan, and W. D. Mooney (2003), Three-dimensional velocity structure of crust and upper mantle in southwestern China and its tectonic implications, *J. Geophys. Res.*, *108*(B9), 2442, doi:10.1029/2002JB001973.

Wang, C., J. Wu, H. Lou, L. Chang, and W. Su (2006), Study on crustal and upper mantle's structure and mantle anisotropy beneath the eastern Tibetan Plateau, *Eos Trans. AGU*, *87*(36), West Pac. Geophys. Meet. Suppl., Abstract S45A-02.

Wdowinski, S., and G. J. Axen (1992), Isostatic rebound due to tectonic denudation: A viscous flow model of a layered lithosphere, *Tectonics*, *11*, 303–312.

Wei, W., et al. (2001), Detection of widespread fluids in the Tibetan crust by magnetotelluric studies, *Science*, *292*, 716–718.

Wernicke, B. P. (1990), The fluid crustal layer and its implications for continental dynamics, in *Exposed Cross Section of the Continental Crust*, edited by M. H. Salisbury and D. M. Fountain, pp. 509–544, Kluwer Acad., Dordrecht, Netherlands.

Xiong, S. B., J. W. Teng, and Z. X. Yin (1986), Explosive seismological research on the structures of crust and upper mantle in the south of Panxi tectonic belt (in Chinese), *Acta Geophys. Sin.*, *29*, 235–244.

Xu, Z. Q., L. W. Hou, and Z. X. Wang (1992), *Orogenic Processes of the Songpan-Garze Orogenic Belt, China* (in Chinese), 60 pp., Geol. Press, Beijing.

Yuan, X. C. (1996), *Geophysics Atlas of China* (in Chinese), pp. 157–158, Geol. Press, Beijing.

Zhang, P. Z., Z. Shen, M. Wang, and W. Gan (2004), Continuous deformation of the Tibetan Plateau from global positioning system data, *Geology*, *32*, 809–812.

Zhao, W. J., K. D. Nelson, and Project INDEPTH Team (1993), Deep seismic reflection evidence for continental underthrusting beneath southern Tibet, *Nature*, *366*, 557–559.

Zhao, Z., and R. S. Zhang (1987), Preliminary study on crustal and upper mantle velocity structure of Sichuan province (in Chinese), *Acta Seismol. Sin.*, *9*, 154–165.

W. W. Chan, Multimax Inc., 13665 Dulles Technology Drive, Suite 250, Herndon, VA 20171, USA. (winston@multimax.com)

W.-B. Han, Sichuan Seismological Bureau, Chengdu 610041, China.

H. Lou, C.-Y. Wang, and J.-P. Wu, Institute of Geophysics, China Seismological Bureau, Beijing 100081, China. (wangcy@cea-igp.ac.cn)